# Activation and Two Modes of Blockade by Strontium of $Ca^{2+}$-activated $K^+$ Channels in Goldfish Saccular Hair Cells

Izumi Sugihara

From the Department of Physiology, Tokyo Medical and Dental University School of Medicine, Tokyo 113, Japan

ABSTRACT Effects of internal $Sr^{2+}$ on the activity of large-conductance $Ca^{2+}$-activated $K^+$ channels were studied in inside-out membrane patches from goldfish saccular hair cells. $Sr^{2+}$ was approximately one-fourth as potent as $Ca^{2+}$ in activating these channels. Although the Hill coefficient for $Sr^{2+}$ was smaller than that for $Ca^{2+}$, maximum open-state probability, voltage dependence, steady state gating kinetics, and time courses of activation and deactivation of the channel were very similar under the presence of equipotent concentrations of $Ca^{2+}$ and $Sr^{2+}$. This suggests that voltage-dependent activation is partially independent of the ligand. Internal $Sr^{2+}$ at higher concentrations (>100 μM) produced fast and slow blockade both concentration and voltage dependently. The reduction in single-channel amplitude (fast blockade) could be fitted with a modified Woodhull equation that incorporated the Hill coefficient. The dissociation constant at 0 mV, the Hill coefficient, and *zd* (a product of the charge of the blocking ion and the fraction of the voltage difference at the binding site from the inside) in this equation were 58–209 mM, 0.69–0.75, 0.45–0.51, respectively ($n = 4$). Long shut events (slow blockade) produced by $Sr^{2+}$ lasted ~10–200 ms and could be fitted with single-exponential curves (time constant, $\tau_{l-s}$) in shut-time histograms. Durations of burst events, periods intercalated by long shut events, could also be fitted with single exponentials (time constant, $\tau_b$). A significant decrease in $\tau_b$ and no large changes in $\tau_{l-s}$ were observed with increased $Sr^{2+}$ concentration and voltage. These findings on slow blockade could be approximated by a model in which single $Sr^{2+}$ ions bind to a blocking site within the channel pore beyond the energy barrier from the inside, as proposed for $Ba^{2+}$ blockade. The dissociation constant at 0 mV and *zd* in the Woodhull equation for this model were 36–150 mM and 1–1.8, respectively ($n = 3$).

KEY WORDS: potassium channels • patch clamp • barium • calcium • block

## INTRODUCTION

Various kinds of cellular processes that are mediated by $Ca^{2+}$ under ordinary conditions can also be activated by $Sr^{2+}$. A classic example is the generation of calcium action potential by $Sr^{2+}$ (Fatt and Ginsborg, 1958). Other examples are transmitter release at a neuromuscular junction (Dodge et al., 1969), uncoupling of electrotonic synapses (Baux et al., 1978), and maintenance of mechano-electrical transduction in hair cells (Ohmori, 1985). Activation of $Ca^{2+}$-activated $K^+$ channels is also known to be produced by $Sr^{2+}$ (McManus and Magleby, 1984; Sugihara and Furukawa, 1986; Oberhauser et al., 1988; Yoshida et al., 1991).

The biophysical properties of large-conductance $Ca^{2+}$-activated $K^+$ channels (BK channels)[1] have been extensively studied in cultured rat skeletal muscle (Barrett et al., 1982; Magleby and Pallotta, 1983*a*; Ferguson, 1991) and in mammalian skeletal muscle T-tubule membrane incorporated into lipid bilayers (Moczydlowski and Latorre, 1983; Vergara and Latorre, 1983; Oberhauser et al., 1988). Similar BK channels have been studied in many types of cells (Marty, 1981; Benham et al., 1985; Lang and Ritchie, 1990; Sugihara, 1994; reviewed by Latorre et al., 1989). Two different blocking effects produced by divalent cations have been reported in BK channels. One is fast blockade, which appears as a reduction in the amplitude of single-channel current, and has been studied in detail for $Mg^{2+}$ (Ferguson, 1991). The other is slow blockade, which appears as the production of long shut events, and has been extensively studied for $Ba^{2+}$ (Vergara and Latorre, 1983; Benham et al., 1985; Miller et al., 1987; Diaz et al., 1996; Neyton, 1996). Fast blockade is also produced by other divalent cations such as $Ca^{2+}$, $Sr^{2+}$, and $Ni^{2+}$ (Marty, 1981; Oberhauser et al., 1988; Ferguson, 1991). Slow blockade is relatively specific to $Ba^{2+}$, although it has been reported that $Sr^{2+}$, $Pb^{2+}$, and $Cd^{2+}$ may also produce slow blockade (Oberhauser et al., 1988). These previous findings suggest that $Sr^{2+}$ is a rather special ion for BK channels in that it can produce activation, fast blockade, and slow blockade.

The purpose of this study was to investigate the properties of BK channels of goldfish hair cells, particularly with regard to activation and blockade by analyzing the

Address correspondence to Dr. Izumi Sugihara, Department of Physiology, Tokyo Medical and Dental University, School of Medicine, 1-5-45 Yushima, Bunkyo-ku, Tokyo 113, Japan. Fax: 81-3-5803-5155; E-mail: isugihara.phy1@med.tmd.ac.jp

[1] *Abbreviation used in this paper:* BK channel, large-conductance $Ca^{2+}$-activated $K^+$ channel.


J. Gen. Physiol. © The Rockefeller University Press • 0022-1295/98/02/363/17 $2.00
Volume 111 February 1998 363–379
http://www.jgp.org

effects produced by $Sr^{2+}$. Regarding general characteristics, such as unitary conductance and $Ca^{2+}$ and voltage sensitivity, BK channels in goldfish hair cells are largely similar to those in many other preparations, although they do have some unique characteristics, such as short open times, low sensitivity to $Ca^{2+}$, and variation in conductance and gating kinetics among channels (Sugihara, 1994). Comparison of the effects of $Sr^{2+}$ and $Ca^{2+}$ on activation contributed to understanding of the activation mechanism. The fast and slow blockades produced by $Sr^{2+}$ were then analyzed in detail. The effects of $Ba^{2+}$ were also analyzed for comparison with $Sr^{2+}$-induced slow blockade. Slow blockade produced by $Sr^{2+}$ was similar to but simpler than that produced by $Ba^{2+}$, and thus the former could be useful for understanding blockade and permeation in BK channels.

## MATERIALS AND METHODS

### *Preparation and Experiments*

The methods for dissociating single hair cells from the inner ear of goldfish, *Carassius auratus*, and for the setup of patch-clamp experiments (Hamill et al., 1981) have been described previously (Sugihara and Furukawa, 1989, 1995, 1996; Sugihara, 1994). Goldfish were anaesthetized with an intramuscular injection of ketamine hydrochloride (1 mg/g body weight$^{-1}$). The dorsal skull and brain were removed to excise the inner ears. Hair cells were isolated from the saccular maculae. All experiments were performed at room temperature (19–22°C). The recording chamber was first filled with normal Ringer's solution containing (mM) 120 NaCl, 2 KCl, 2 $CaCl_2$, 5 Hepes, 1.5 NaOH, pH 7.2. When the patch pipette was placed in the bath, a small constant voltage was applied to the pipette to obtain zero current. After the formation of a gigaohm seal in the basolateral surface of the cell, the pipette voltage was shifted by the value of the liquid junctional voltage (−4 mV KCl solution [see below] in the pipette against normal Ringer's solution bath), which should hereafter be absent. The bath of normal Ringer's solution was then replaced with 125 mM KCl solution, and the cell, except for the membrane patch, was destroyed by being hit with a small air bubble to form an inside-out patch (Sugihara, 1994). To identify BK channels, membrane current was monitored while the bath solution was changed from $Ca^{2+}$-free KCl to KCl with an internal calcium concentration ($[Ca^{2+}]_i$) of 5 μM and to NaCl (125 mM) with 5 μM $[Ca^{2+}]_i$, and then back to KCl. Experiments were performed with membrane patches in which one or a few BK channels (>150 pS) were detectable. Membrane patches in which a single BK channel was present were used in experiments to measure open and shut times or reductions in the unitary amplitude. The seal resistance of the membrane patch was >10 GΩ.

### *Data Analysis*

Data acquisition and analysis were facilitated by the use of various custom programs developed in the laboratory. The output of the patch-clamp amplifier (10-kHz three-pole low-pass filter, EPC7; List Electronic, Darmstadt, Germany) was recorded with a PCM data recorder (PR-880; NF Electronic Instruments, Yokohama, Japan) at a sampling interval of 17.4 μs. The replayed data or the direct output of the amplifier was then passed through a low pass four-pole Bessel filter (DT-408; NF Electronic Instruments), digitized, and stored on the hard disk of a microcomputer (N10; Nippon Data General, Tokyo, Japan, or PC-9801RA; NEC, Tokyo, Japan) for analysis. The cut-off frequency was 10 kHz (−3 dB; 24 dB/octave) and the sampling interval for digitizing was 20 μs. Continuous acquisition of data of unlimited length was possible with this digitizing speed until the hard disk became full.

Open state probability ($P_o$) and mean open and shut times were calculated from a continuous record of 3–5 s. $P_o$ was measured as the fraction of time in which the current exceeded 50% of the open amplitude (Barrett et al., 1982). The open and shut times were defined as the time between a shut–open and the next open–shut transition and the time between an open–shut and the next shut–open transition, respectively. The threshold for shut–open and open–shut transitions was set at 0.5 of the unitary current amplitude. Mean open and shut times were calculated as arithmetic averages of the duration of the open and shut times.

To analyze the time course of activation and deactivation, voltage pulses (17 ms in duration) were repeatedly applied to the membrane patch every 1.3 s. Successive records, 100–400 in number, were averaged after leakage and capacitive currents had been subtracted. Leakage and capacitive currents were measured from records with no open events or from records in response to negative voltage steps. To measure the time constants of activation and deactivation, single-exponential curves that fit the rising or decay phase of the current record were obtained using the maximum likelihood method with Simplex minimization (Dempster, 1993).

To measure the unitary amplitude, an amplitude histogram was plotted from a single channel current record of ~320 ms, and a pair of Gaussian curves that fit the shut and open levels were obtained using the binned maximum likelihood method with Simplex minimization (Dempster, 1993). The unitary amplitude was measured from the difference of the means of the two Gaussian curves.

Distributions of open and shut times were calculated from three to tens of seconds of continuous records of single-channel currents to analyze gating under activation by $Sr^{2+}$ or $Ca^{2+}$. Much longer records (e.g., extending for more than 100 s and containing 32,000–2,000,000 consecutive open and shut events) were used to analyze slow blockade. Histograms of open and shut times were plotted with a logarithmic time axis and a square-root ordinate (Sigworth and Sine, 1987). The bin width used was $\log(2^{0.125}) = \log(1.095)$; i.e., bin No., $n$, was used to count events of duration $x_{min} - x_{max}$ (in integer sampling periods), $2^{0.125n} \leq x_{min}$, $x_{max} < 2^{0.125(n+1)}$. Two to several neighboring bins were combined for very short times of <160 μs; i.e., events with durations of 1, 2, 3, 4, 5, 6, and 7 sampling periods (20 μs) were counted in combined bins 0–7, 8–11, 12–15, 16–17, 18–19, 20–21, and 22–23, respectively. Since the durations of the events were counted as discrete values (i.e., multiples of the digitizing time) in the computer, the width of each bin ($t_1 = 2^{0.125(n+1)} - 2^{0.125n}$) of very short duration in the histogram was different from the actual time range ($t_2 = x_{max} - x_{min} + 1$) counted within that bin. Therefore, the bin count was adjusted by multiplying by $t_1/t_2$. These procedures did not affect the results of the analysis because very short events (<0.5 ms) were not used to calculate the fitting of exponential curves. Histograms in a certain section of time bins were fitted with exponential curves using the binned maximum likelihood method (Sigworth and Sine, 1987; Dempster, 1993) with Simplex minimization (Dempster, 1993). Undersampling of short events due to filtering was not corrected because it was not a serious concern for the relative comparisons shown in Fig. 3 or for the analysis of burst duration shown in Fig. 8. Fitting straight lines were obtained with least-squares methods. In semilog or log–log plots, logarithm values were used to calculate fitting lines.

While recording the channel activity for long periods of time, transient shifts of the gating mode (McManus and Magleby, 1988; Sugihara, 1994) were occasionally observed. These shifts were of different types. In one type, very short bursts (<100 μs) composed of a single or a few open events occurred repetitively. The shut states that intercalated these very short bursts were either of medium duration (10–500 ms) or were very long (>500 ms). In another type of shift, a reduction of the single-channel amplitude (to 42%) accompanied the shortening of shut times. The occurrence of these shifts in the gating mode did not seem to be affected by increases in $[Sr^{2+}]_i$ or the membrane voltage. The time during which a channel showed a shift in the gating mode was <10% of the recording time. Periods of transient shifts in gating were simply omitted for the analysis of slow blockade by $Sr^{2+}$.

### *Solutions*

For recordings in the inside-out mode, the pipette (external) solution was composed of 125 mM KCl and 5 mM Hepes (pH adjusted to 7.2 with ~1.5 mM KOH). The bath (internal) solution was composed of 125 mM KCl and 5 mM Hepes (pH adjusted to 7.2 with ~1.5 mM KOH), plus a given concentration of $SrCl_2$, $CaCl_2$, or $MgCl_2$ (all from Wako Chemicals, Osaka, Japan). For $Ca^{2+}$ concentrations of 2 μM or less, EGTA and $CaCl_2$ were added to the 125-mM KCl solution in ratios calculated according to Barrett et al. (1982) to give the final desired free concentration. For $Ca^{2+}$ concentrations of 5 μM or higher, EGTA was not included in the solution. $Ca^{2+}$ contamination in nominally Ca-free KCl solution was found to be ~0.5 μM by comparing the open state probabilities of BK channels in inside-out patches bathed in nominally $Ca^{2+}$-free and Ca-EGTA solutions (Sugihara, 1994). The BK channels in goldfish hair cells are scarcely activated by 0.5 μM $Ca^{2+}$, even at +50 mV (Sugihara, 1994). Contamination by Ca in $SrCl_2$ is <0.03%. This contamination by $Ca^{2+}$ was ignored in the analyses of activation because $Sr^{2+}$ was approximately one-fourth as potent as $Ca^{2+}$ in activating BK channels (see RESULTS). Contamination by Ba in $SrCl_2$ is <0.02%. This equals <2 μM $Ba^{2+}$ in 10 mM $Sr^{2+}$ solution. The ability of 2 μM $Ba^{2+}$ to produce a slow blocked state is much smaller than that of 10 mM $Sr^{2+}$, and in fact is nearly negligible. Therefore, $Ba^{2+}$ contamination was ignored in the analyses of slow blockade produced by $Sr^{2+}$. When the internal solution in the bath was to be exchanged, 200 ml of the solution was superfused to completely wash the content of the chamber (~2 ml).

## RESULTS

### *Activation of BK Channels by $Sr^{2+}$*

$Sr^{2+}$ activated BK channels in goldfish hair cells in a voltage- and concentration-dependent manner. The records of the steady state activities of two BK channels (conductance, 308 pS) in an inside-out membrane patch (Fig. 1) show that channels did not open at −20 mV with an internal $Sr^{2+}$ concentration ($[Sr^{2+}]_i$) of 2 μM, while opening was readily observed at −20 mV with 10 μM $[Sr^{2+}]_i$. At all of the $[Sr^{2+}]_i$ levels, the frequency of opening was markedly enhanced by depolarization of the membrane voltage from −20 (Fig. 1, *middle* and *bottom*) to +50 mV (Fig. 1, *top*). Increased $[Sr^{2+}]_i$ also facilitated opening of the channel at each voltage.

$P_o$ was measured for a wide range of $[Sr^{2+}]_i$ values at different membrane voltages for the same membrane patch (Fig. 2 *A*). Occasional long shut events longer than 20 ms were omitted from this measurement when $[Sr^{2+}]_i$ was higher than 200 μM and the membrane voltage was higher than 0 mV since they were likely to reflect slow blocked states (see below). $P_o$ increased with an increase in $[Sr^{2+}]_i$, as well as with an increase in the membrane voltage (Fig. 2 *A*). $P_o$ measured under activation by $Ca^{2+}$ (at 50 mV) in the same membrane patch was also plotted (Fig. 2 *A*, □). The plots for $Sr^{2+}$ were shifted rightward to a higher concentration than that for $Ca^{2+}$ at the same membrane voltage, but the maximum $P_o$ ($P_{oMAX}$) was the same for $Sr^{2+}$ and $Ca^{2+}$ (~0.91 in this case, Fig. 2 *A*). Fast flickering gating persisted at a saturation level of $Sr^{2+}$ activation so that $P_{oMAX}$ never reached 1, as was found for $Ca^{2+}$ activation in BK channels of goldfish hair cells (Sugihara, 1994). The Hill coefficient for activation by $Sr^{2+}$ was larger for positive than for negative voltages (1.6 at 50 mV, ~0.7

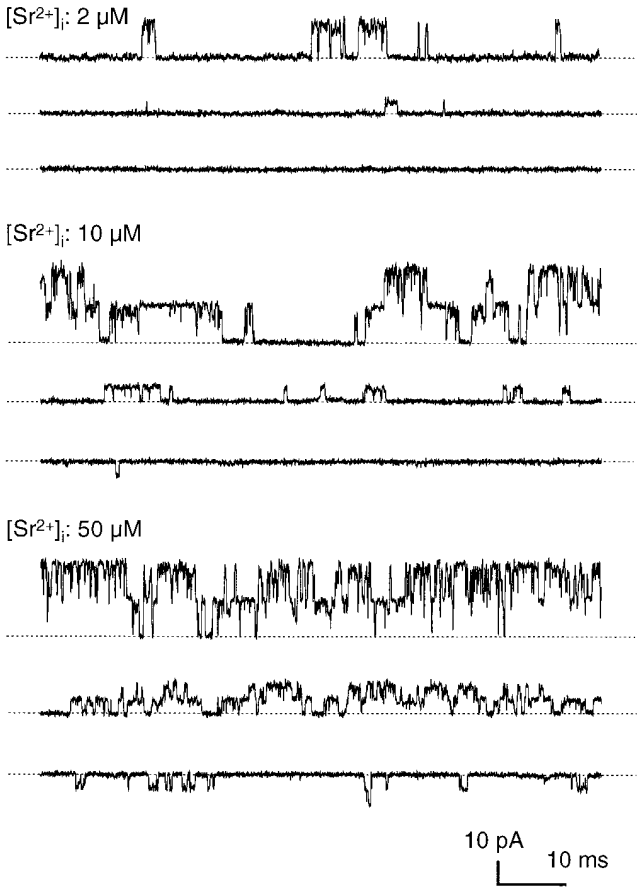


FIGURE 1. Activation of BK channels by $Sr^{2+}$. Sample records obtained from an inside-out membrane patch that had two 308-pS BK channels at different $[Sr^{2+}]_i$ (2, 10, and 50 μM). Membrane voltage is 50, 20, and −20 mV from top to bottom in each set.

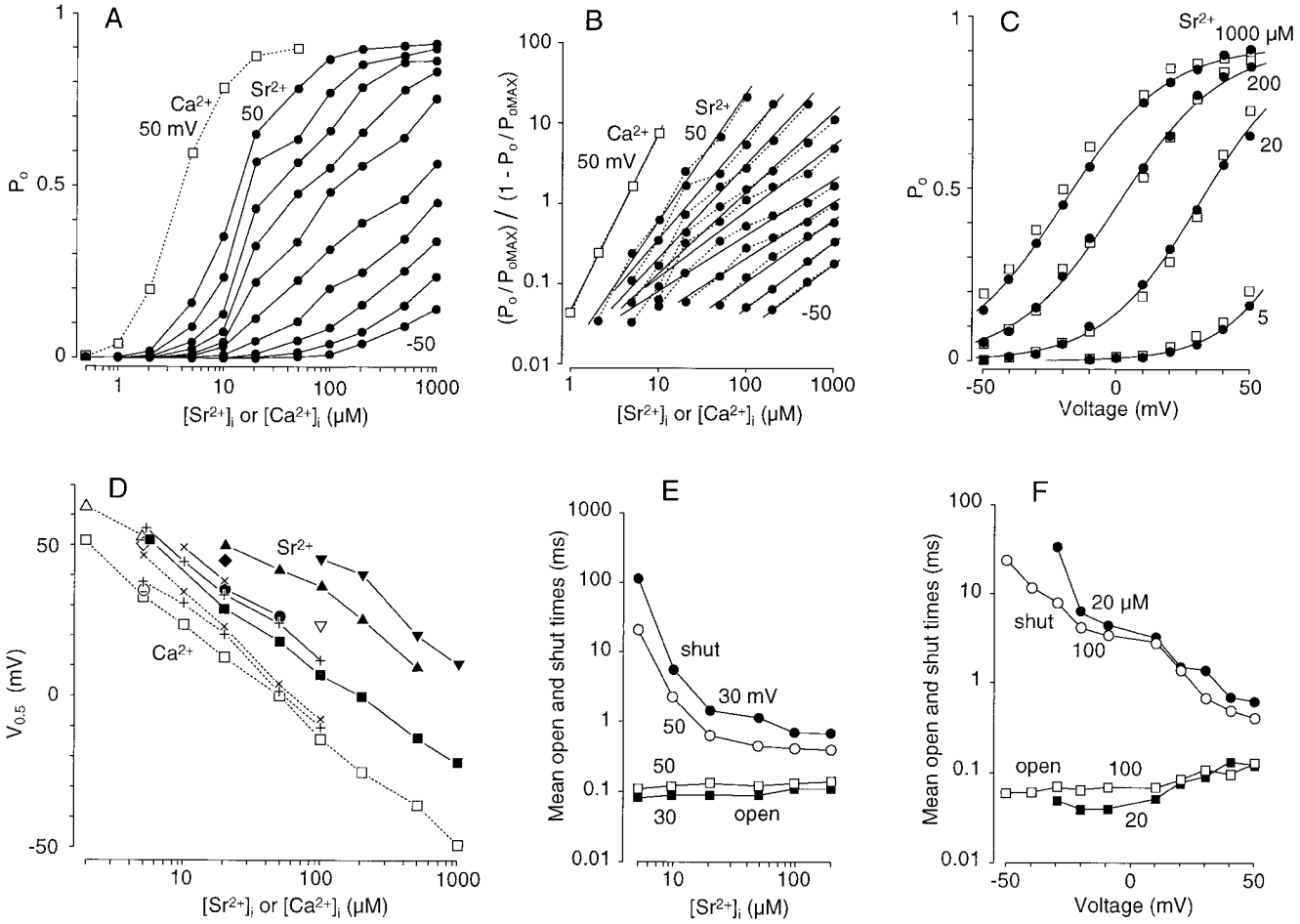


FIGURE 2. Analysis of $Sr^{2+}$-induced activation of BK channels. (*A*) Dose–response curves. $P_o$ is plotted against $[Sr^{2+}]_i$ (●) for different membrane voltages (50 to 10 and −10 to −50 mV from top to bottom). For comparison, $P_o$ measured with $Ca^{2+}$ at 50 mV is also shown (□ and *dotted lines*). (*B*) Hill plots of BK channel activation. $(P_o/P_{oMAX})/(1 - P_o/P_{oMAX})$ is plotted against $[Sr^{2+}]_i$ (●) and $[Ca^{2+}]_i$ (□) on a log–log scale for the data shown in *A*. The slopes are 1.6, 1.3, 1.2, 1.0, 0.83, 0.69, 0.70, 0.79, 0.78, and 0.72 for $Sr^{2+}$ (+50 to −50 mV) and 2.7 for $Ca^{2+}$ (50 mV). $P_{oMAX} = 0.91$. (*C*) $P_o$ is plotted against membrane voltage for activation by $Sr^{2+}$ (●, 1,000, 200, 20, and 5 µM from left to right) and $Ca^{2+}$ (□, 200, 50, 5, and 1 µM from left to right). S-shaped curves were drawn using a Boltzmann distribution to fit the plots for each $[Sr^{2+}]_i$, $V_{0.5}$ and *n* of which were −22 mV and 1.3, 1 mV and 1.3, 39 mV and 1.4, and 72 mV and 1.6, respectively, from left to right. Plots in *A*, *B*, and *C* were obtained in the membrane patch used in Fig. 1. (*D*) The half-activation voltage, $V_{0.5}$, which was obtained from a Boltzmann distribution, is plotted against $[Sr^{2+}]_i$ (*symbols filled or connected with straight lines*) and $[Ca^{2+}]_i$ (*symbols open or connected with dotted lines*) for eight membrane patches, each containing one or two BK channels. Symbols of the same shape indicate the same membrane patch. (*E*) Mean open (*squares*) and shut (*circles*) times measured in a BK channel at 30 (*filled*) and 50 (*open*) mV are plotted against $[Sr^{2+}]_i$. (*F*) Mean open (*squares*) and shut (*circles*) times measured in a BK channel at 20 (*filled*) and 100 (*open*) µM $[Sr^{2+}]_i$ are plotted against membrane voltage.

between −10 and −50 mV; Fig. 2 *B*). A similar tendency was observed for $Ca^{2+}$ activation (Sugihara, 1994). The Hill coefficient for $Ca^{2+}$ was larger than that for $Sr^{2+}$ at the same voltage (2.7 and 1.6 for $Ca^{2+}$ and $Sr^{2+}$, respectively, at 50 mV; Fig. 2 *B*). This was also reflected in the maximum slope of each concentration–$P_o$ curve, which was less steep for $Sr^{2+}$ than for $Ca^{2+}$ at 50 mV (Fig. 2 *A*).

When $P_o$ was plotted against the membrane voltage for different $[Sr^{2+}]_i$ (Fig. 2 *C*), the resulting S-shaped relations could be roughly fitted with a Boltzmann distribution:

$$P_o(V)/P_{oMAX} = \{1 + \exp[-nF(V - V_{0.5})/(RT)]\}^{-1}, \quad (1)$$

where $P_{oMAX}$ is the saturated value of $P_o$, *n* is a constant representing the equivalent number of gating charges, $V_{0.5}$ is the membrane voltage at which $P_o$ is 1/2 of $P_{oMAX}$, V is the applied voltage, and *F*, *R*, and *T* have their usual meanings. *RT*/*F* is 25.4 mV at 22°C. The *n* value for the Boltzmann distribution used to fit the plots for 10–1,000 µM $[Sr^{2+}]_i$ ranged between 1.3 and 1.6 (see legend for Fig. 2 *C*). The *n* value was slightly larger for smaller $[Sr^{2+}]_i$ as found for $[Ca^{2+}]_i$ in the

cloned BK channel (Cui et al., 1997). The plots for $Ca^{2+}$ obtained from the same membrane patch had a similar S-shape and were nearly identical to the plots for $Sr^{2+}$ at certain higher concentrations; for example, the plot for 50 μM $[Ca^{2+}]_i$ was nearly identical to that for 200 μM $[Sr^{2+}]_i$, showing that these are equipotent concentrations. Values of $n$ in six other membrane patches were between 1.3 and 2.1 and were similar for $Ca^{2+}$ (5 μM) and $Sr^{2+}$ (20–100 μM) in each case. These results indicate that the voltage dependence of a BK channel activated by $Ca^{2+}$ is indistinguishable from that activated by $Sr^{2+}$ as long as equipotent concentrations of $Ca^{2+}$ and $Sr^{2+}$ are used to activate the channel to a similar degree. The $n$ values obtained in the present channel were similar to those obtained in rat skeletal muscle (∼2.0, Oberhauser et al., 1988) and in the *mslo* BK channel (1.1–1.8, Cui et al., 1997).

To compare the potencies of $Sr^{2+}$ and $Ca^{2+}$ in activating BK channels, $V_{0.5}$ was measured in eight membrane patches in voltage–$P_o$ plots under several different $Sr^{2+}$ and $Ca^{2+}$ concentrations (Fig. 2 *D*). The slopes of the concentration–$V_{0.5}$ plots indicated that a 10-fold increase in $[Sr^{2+}]_i$ and $[Ca^{2+}]_i$ produced an ∼25- and 35-mV decrease in $V_{0.5}$, respectively. The concentration–$V_{0.5}$ plots for $Sr^{2+}$ were shifted rightward by approximately fourfold from those for $Ca^{2+}$ in all cases, indicating that $Sr^{2+}$ was approximately one-fourth as potent as $Ca^{2+}$ (Fig. 2 *D*). This difference in potency was greater at higher concentrations of $[Sr^{2+}]_i$ and $[Ca^{2+}]_i$ due to the different slopes of the plots (Fig. 2 *D, squares*). This is related to the finding that the Hill coefficient for $Sr^{2+}$ is smaller than that for $Ca^{2+}$ (Fig. 2 *B*). Flattening of concentration–$V_{0.5}$ plots at high (50–1,000 μM) $[Ca^{2+}]_i$ (Wei et al., 1994; Cui et al., 1997) or $[Sr^{2+}]_i$ was not obvious in the present experiments.

Mean open and shut times were plotted against $[Sr^{2+}]_i$ and membrane voltage in a membrane patch with a single BK channel (Fig. 2, *E* and *F*) to examine the effects of $Sr^{2+}$ on the gating of BK channels. The decrease in the mean shut time was much greater than the increase in the mean open time when the channel was activated by increased $[Sr^{2+}]_i$ or membrane voltage. This is similar to the changes that occur when the channel is activated by $Ca^{2+}$ (Sugihara, 1994).

The distributions of open and shut times were calculated to further examine the difference in the gating of the BK channel activated by $Ca^{2+}$ and $Sr^{2+}$. 5 μM $[Ca^{2+}]_i$ and 20 μM $[Sr^{2+}]_i$ produced similar $P_o$ values (0.309 and 0.315 for $Sr^{2+}$ and $Ca^{2+}$, respectively, at 50 mV) in the BK channel shown in Fig. 3, indicating that

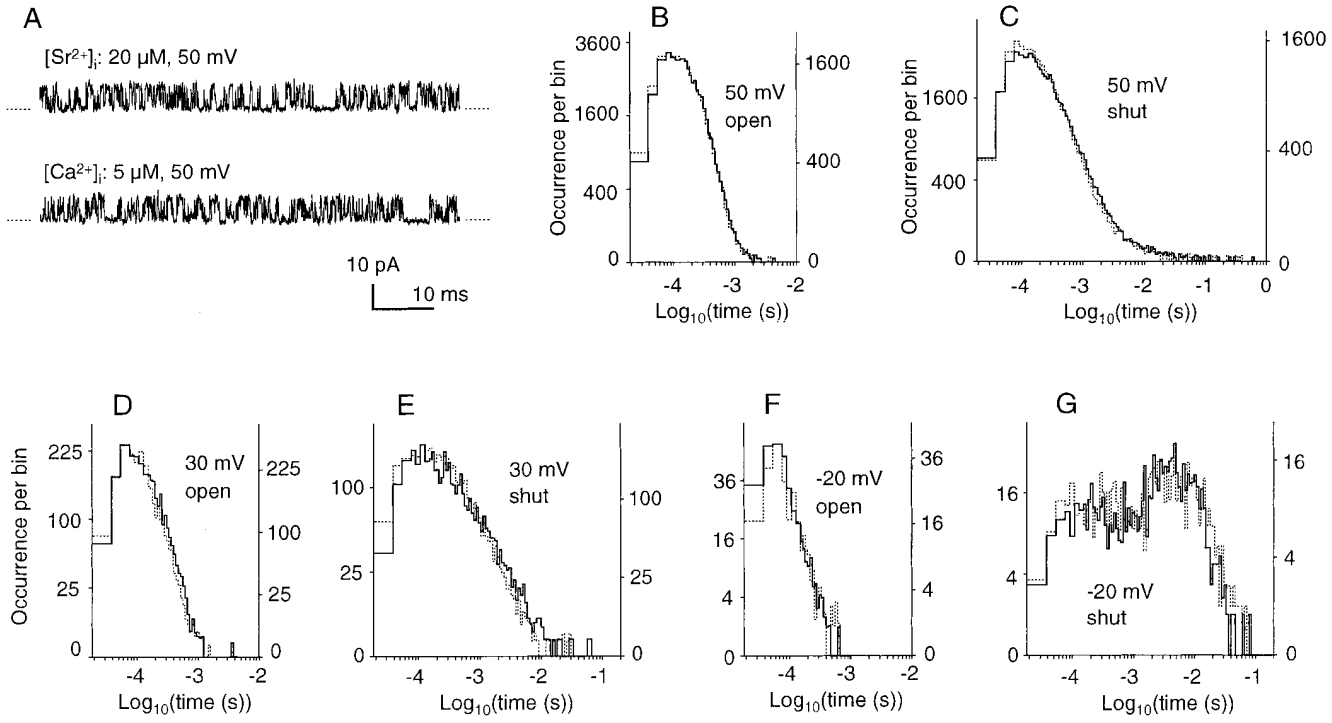


FIGURE 3. Open- and shut-time distributions of a BK channel activated by $Sr^{2+}$ and $Ca^{2+}$. (*A*) Sample traces. Recorded at +50 mV with 20 μM $[Sr^{2+}]_i$ (*top*) or 5 μM $[Ca^{2+}]_i$ (*bottom*). (*B–G*) Open- (*B, D,* and *F*) and shut- (*C, E,* and *G*) time distributions for 20 μM $[Sr^{2+}]_i$ (*solid line* and *left ordinate*) and 5 μM $[Ca^{2+}]_i$ (*dotted line* and *right ordinate*) at the membrane potentials indicated in the figure. Two histograms were superimposed on each other using different ordinate scales. Recording times and total number of events: 43 s and 163,160 ($Sr^{2+}$, 50 mV), 23 s and 94,500 ($Ca^{2+}$, 50 mV), 3.9 s and 11,097 ($Sr^{2+}$, 30 mV), 3.5 s and 13,689 ($Ca^{2+}$, 30 mV), 4.5 s and 2,149 ($Sr^{2+}$, −20 mV), and 3.9 s and 1,637 ($Ca^{2+}$, −20 mV).

these concentrations of $Sr^{2+}$ and $Ca^{2+}$ were equipotent in this channel. The steady state activities recorded with 20 μM $Sr^{2+}$ and 5 μM $Ca^{2+}$ at 50 mV were almost the same (Fig. 3 *A*). Distributions of open and shut times obtained from long records under these conditions are shown in Fig. 3, *B* and *C*. While the open-time distributions were rather simple, with a peak at ~0.1 ms (Fig. 3 *B*), the shut-time distributions had a wide distribution due to some long shut events of 10–600 ms in duration (Fig. 3 *C*). The histograms for $Sr^{2+}$ and $Ca^{2+}$ were nearly identical to each other for both open and shut times, including the above points. Similarly, the open and shut time distributions obtained at different membrane voltages with the same $[Sr^{2+}]_i$ and $[Ca^{2+}]_i$ resembled each other (Fig. 3, *D–G*). Similar findings were observed in three other BK channels.

The time courses of activation and deactivation after voltage steps differ greatly depending on $[Ca^{2+}]_i$ in BK channels (Sugihara, 1994). I examined whether $Sr^{2+}$ and $Ca^{2+}$ produce different time courses of activation and deactivation. Current records from a single BK channel in response to voltage steps from the holding voltage of −50 to +50 mV were averaged to investigate the time courses of activation and deactivation under the presence of 20 μM $Sr^{2+}$ or 5 μM $Ca^{2+}$ (Fig. 4). These concentrations of $Sr^{2+}$ and $Ca^{2+}$ produced roughly similar activation in the steady state in this BK channel. There was no clear difference in the responses of channel activity seen in the current traces for $Sr^{2+}$ and $Ca^{2+}$ (Fig. 4, *A, a* and *B, a*). The time courses of the average current for $Sr^{2+}$ and $Ca^{2+}$ resembled each other (Fig. 4, *A, b* and *B, b*). The activation time constants (1.22 and 1.14 ms) and deactivation time constants (0.61 and 0.54 ms) for $Sr^{2+}$ and $Ca^{2+}$ were close to each other, indicating that the time courses of activation and deactivation for equipotent $Sr^{2+}$ and $Ca^{2+}$ were nearly identical. Similar results were obtained in another experiment.

These results showed that while $Sr^{2+}$ and $Ca^{2+}$ differ with regard to potency and the Hill coefficient in activating the channel, equipotent concentrations of these divalent cations produce nearly identical activity in BK channels. Remarkable similarity was demonstrated with regard to $P_{oMAX}$, voltage dependence of activation, steady state gating kinetics, and the time courses of voltage-dependent activation and deactivation. Note that the above analysis of activation was performed mainly at relatively low $[Sr^{2+}]_i$, and that the production of slow blocked events at high $[Sr^{2+}]_i$ was not addressed in this section.

### *Fast Blockade of BK Channels by $Sr^{2+}$*

Unitary current amplitude of the BK channel is nearly linearly related to the membrane voltage in the voltage

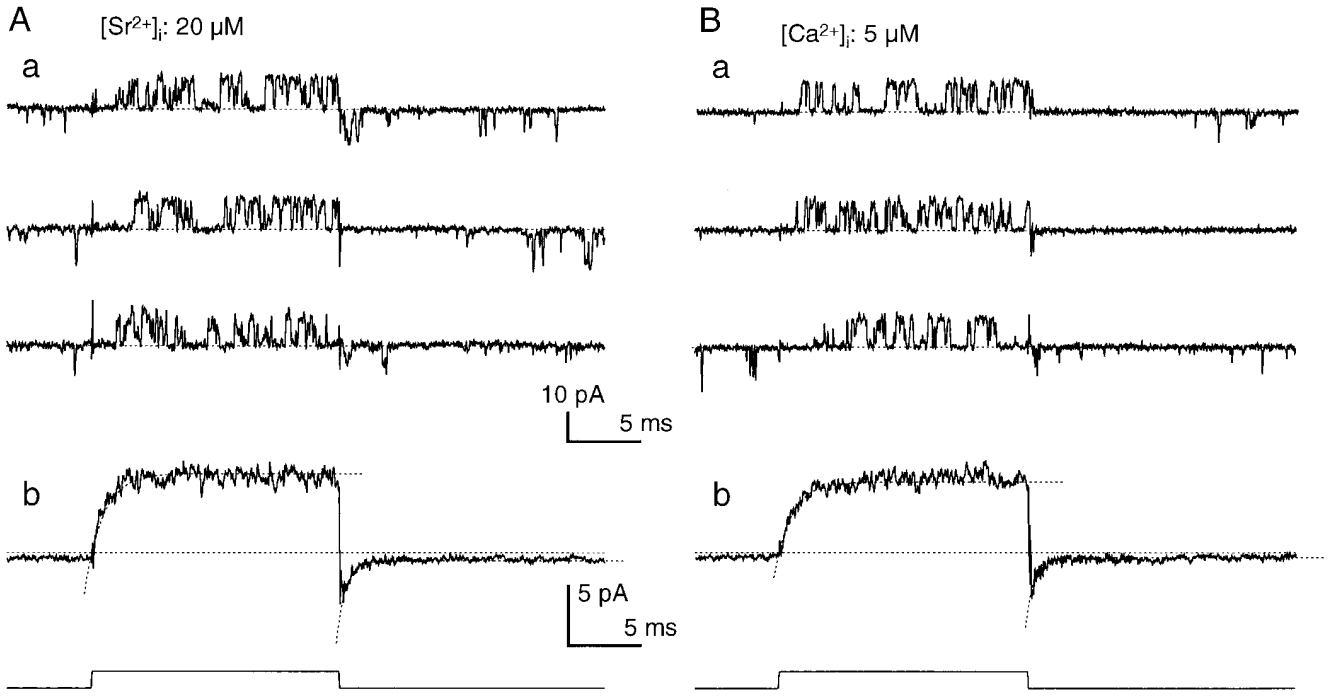


FIGURE 4. Response of a single BK channel to voltage steps under the presence of $Sr^{2+}$ or $Ca^{2+}$. (*A* and *B*) Three sample records (*a*) and the average trace (*b*) under the presence of 20 μM $[Sr^{2+}]_i$ (*A*) and 5 μM $[Ca^{2+}]_i$ (*B*). Number of traces used to obtain the average: 100 and 160 in *A* and *B*, respectively. The time constants of single-exponential curves that fit the activation and tail-decay time courses (*dotted curves*) were 1.22 and 0.61 ms, respectively, in *A*, and 1.14 and 0.54 ms, respectively, in *B*.

range between −50 and +100 mV when activated by low $[Ca^{2+}]_i$ (Sugihara, 1994). This was also true when the channel was activated by low $[Sr^{2+}]_i$ (5–20 μM), and single-channel conductances under activation by $Ca^{2+}$ and $Sr^{2+}$ were identical. Under higher $[Sr^{2+}]_i$, however, the current amplitude deviated from the original linear relation in a voltage- and concentration-dependent manner (Fig. 5). In the case shown in Fig. 5, the original single-channel current amplitude was 13.2 and 26.1 pA at 50 and 100 mV, respectively, with 5 μM $[Ca^{2+}]_i$. Corresponding values for 0.1, 1.0, and 10 mM $[Sr^{2+}]_i$ were 12.3 and 23.7, 10.9 and 19.7, and 8.0 and 9.8 pA, respectively. Thus, the reduction was greater with higher $[Sr^{2+}]_i$ and at larger membrane voltage. The amplitudes measured in the same channel at several voltages and $[Sr^{2+}]_i$ are plotted in Fig. 6 *A*. Since there was no shift in the reversal voltage in the current–voltage relation in Fig. 6 *A*, it could be concluded that, while it produced fast blockade, $Sr^{2+}$ could scarcely permeate the channel. Since there was no apparent increase in the noise level in the current during open events (Fig. 5, *G* and *H*), the blockade should be very fast.

Ferguson (1991) has shown that Woodhull equation (Woodhull, 1973) fits the voltage-dependent reduction in current amplitude in BK channels in mammalian cultured skeletal muscle membrane at a given concentration of internal divalent cations ($Mg^{2+}$, $Ca^{2+}$, $Ni^{2+}$, $Sr^{2+}$), whereas this equation cannot reflect concentration-dependent reduction without changing the value

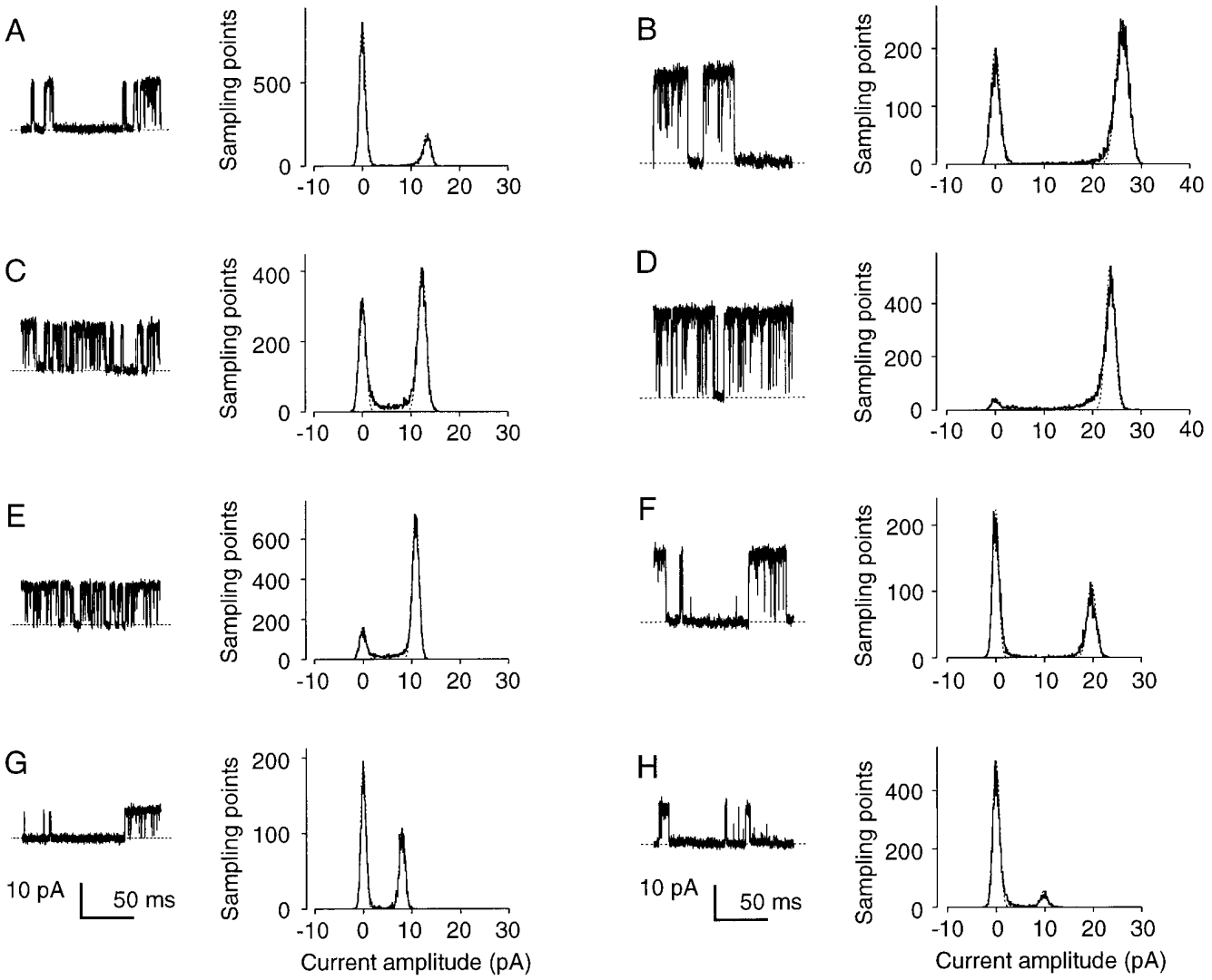


FIGURE 5. Concentration- and voltage-dependent reduction in the current amplitude by high $[Sr^{2+}]_i$. (*A–F*) Sample records and amplitude histograms obtained from a single BK channel. Ligand concentrations: 5 μM $[Ca^{2+}]_i$ (*A* and *B*), 100 μM $[Sr^{2+}]_i$ (*C* and *D*), 1 mM $[Sr^{2+}]_i$ (*E* and *F*), and 10 mM $[Sr^{2+}]_i$ (*G* and *H*); membrane voltage: 50 (*A, C, E,* and *G*) and 100 (*B, D, F,* and *H*) mV. Dotted straight lines indicate zero-current levels. Dotted curves are fitting Gaussian curves.

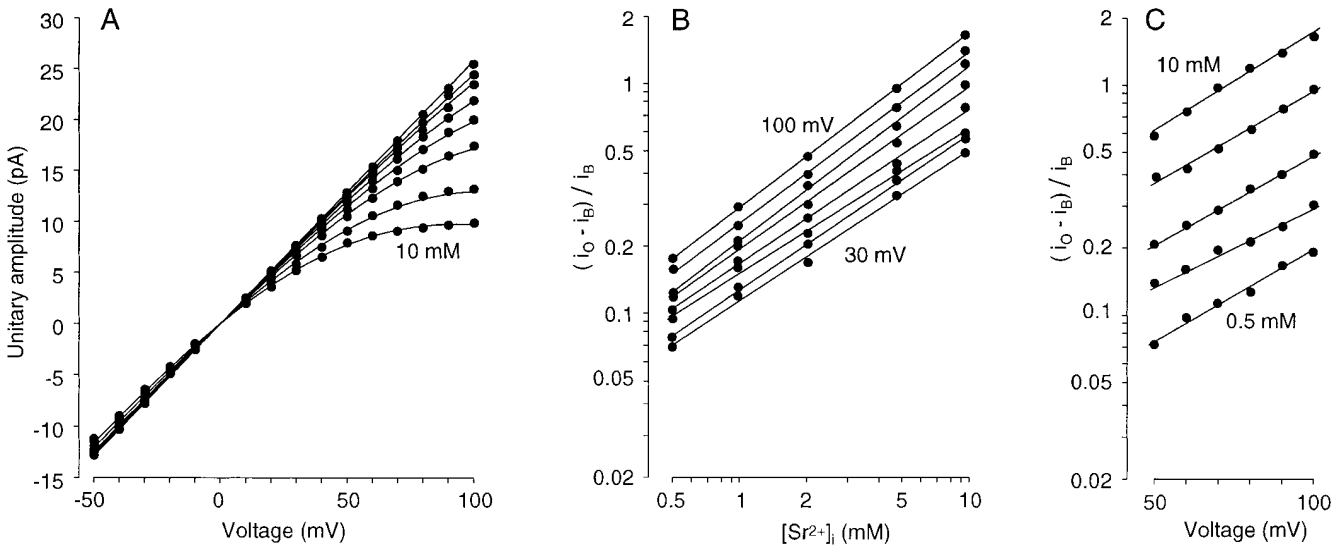


FIGURE 6. Analysis of the concentration- and voltage-dependent reduction in current amplitude by high $[Sr^{2+}]_i$. (*A*) Current–voltage relationship for different $[Sr^{2+}]_i$. Divalent cation concentrations, 5 μM $[Ca^{2+}]_i$, 100, 200, and 500 μM, and 1, 2, 5, and 10 mM $[Sr^{2+}]_i$, from top to bottom on the right side. Single-channel conductance measured from the amplitude at 50 mV with 5 μM $[Ca^{2+}]_i$ (264 pS) was used as a control conductance in further analysis. The fitting curves were drawn according to a modified Woodhull equation with N = 0.74, zd = 0.45, and $K_{d(F)}$ = 58 mM. See text for details. (*B*) Hill plot for amplitude reduction. Membrane voltages, 100–30 mV from top to bottom. Hill coefficients (i.e., slopes of the fitting straight lines) are 0.75, 0.73, 0.75, 0.70, 0.66, 0.62, 0.67, and 0.64 from top to bottom. (*C*) The ratio of the reduction in amplitude, $(i_O - i_B)/i_B$, is plotted against membrane voltage with a logarithmic ordinate. $[Sr^{2+}]_i$ is 10, 5, 2, 1, and 0.5 mM from top to bottom. The slopes of the fitting straight lines are $\log(e^{0.019}\text{-fold})$, $\log(e^{0.018}\text{-fold})$, $\log(e^{0.017}\text{-fold})$, $\log(e^{0.016}\text{-fold})$, and $\log(e^{0.018}\text{-fold})$ $mV^{-1}$, from the top to bottom. In *B* and *C*, data from *A* at positive voltages and high $[Sr^{2+}]_i$ were used.

of the dissociation constant. In the present study, I first made a Hill plot to analyze the concentration-dependent reduction in the unitary current amplitude at each membrane voltage (Fig. 6 *B*). Data obtained at concentrations lower than 0.5 mM or at voltages lower than 30 mV were discarded because scattering became large due to the very small degree of current reduction. The slopes of the fitting straight lines (i.e., Hill coefficients) were ~0.7 for all voltages (0.62–0.75, Fig. 6 *B*).

The reduction in amplitude was then plotted against the voltage (Fig. 6 *C*). The linear relationship of the plots indicated that Woodhull equation could fit the data at each $[Sr^{2+}]_i$:

$$i_O / i_B = 1 + ( [B] / K_{d(F)}(0) ) \exp( zdVF / [RT] ), \quad (2)$$

where $i_O$ and $i_B$ are the amplitudes of single-channel currents in the absence and presence of blocker, respectively, $[B]$ is the concentration of the blocking ion ($Sr^{2+}$ in this case), $K_{d(F)}(0)$ is the dissociation constant of the ion for fast blockade at 0 mV, $z$ is the effective charge in valence of the blocking ion, $d$ is the fraction of the voltage difference at the binding site as measured from the intracellular side of the membrane, and V is the voltage difference across the membrane (Woodhull, 1973). However, Eq. 2 could not fit the data with different $[Sr^{2+}]_i$ without changing $K_{d(F)}(0)$ as in skeletal muscle BK channels (Ferguson, 1991). Therefore, the Woodhull equation was modified by incorporating the Hill coefficient to address the amplitude reduction at different $[Sr^{2+}]_i$:

$$i_O / i_B = 1 + ( [B] / K_{d(F)}(0) )^N \exp( zdVF / [RT] ), \quad (3)$$

where $N$ is the Hill coefficient. The fitting straight lines in Fig. 6 *C* had slopes between $\log(e^{0.019}\text{-fold})$ and $\log(e^{0.016}\text{-fold})$ $mV^{-1}$ (mean, $\log(e^{0.018}\text{-fold})$ $mV^{-1}$), giving a $zd$ value of 0.45. The Hill coefficient obtained from the data was 0.74 (average from plots for 100–80 mV). $K_{d(F)}(0)$ for the best fit was 58 mM. Using these parameters, the modified Woodhull equation (Eq. 3) showed a good fit to the amplitude reduction at all of the $[Sr^{2+}]_i$ values tested (curves in Fig. 6 *A*).

Analyses carried out with high $[Sr^{2+}]_i$ in four membrane patches produced basically similar results (Table I). A Hill coefficient of ~0.7 and a $zd$ value of ~0.5 were obtained in each case. $K_{d(F)}(0)$ was ~60 mM in each case except for one. A channel with a conductance of 178 pS had a larger $K_{d(F)}(0)$ (209 mM) than the others. This variation in the parameters of fast blockade among BK channels in the present study may be related to the nonuniform nature of these BK channels (Sugihara, 1994).

In two experiments, the effects of $Mg^{2+}$ and $Ca^{2+}$ were also measured (Table I, channels three and four). $Mg^{2+}$ and $Ca^{2+}$ produced a reduction in the current

TABLE I

*Parameters for the Modified Woodhull Equation (Eq. 3) Measured in BK Channels*

| Channel | Unitary conductance | Divalent cation | $N$ | $zd$ | $K_{d(F)}(0)$ |
|---|---|---|---|---|---|
| | *pS* | | | | *mM* |
| 1 | 262 | $Sr^{2+}$ | 0.74 | 0.45 | 58 |
| 2 | 224 | $Sr^{2+}$ | 0.75 | 0.51 | 60 |
| 3 | 250 | $Sr^{2+}$ | 0.73 | 0.48 | 63 |
| | | $Ca^{2+}$ | 0.68 | 0.50 | 46 |
| | | $Mg^{2+}$ | 0.71 | 0.50 | 39 |
| 4 | 178 | $Sr^{2+}$ | 0.69 | 0.45 | 209 |
| | | $Ca^{2+}$ | 0.66 | 0.41 | 126 |
| | | $Mg^{2+}$ | 0.70 | 0.47 | 105 |

amplitude very similar to that produced by $Sr^{2+}$. While the values of N and *zd* were similar to those for $Sr^{2+}$ (Table I), the $K_{d(F)}(0)$ values were slightly different among the divalent cations. The order of the potency of these divalent cations, as represented by the reciprocal of $K_{d(F)}(0)$, was $Mg^{2+} > Ca^{2+} > Sr^{2+}$. While high $[Sr^{2+}]_i$ produced frequent long shut events (see below), $Mg^{2+}$ and $Ca^{2+}$ produced such events infrequently. Therefore, 5–10 μM $Ba^{2+}$ was added to the internal (bath) solution in these experiments to facilitate the measurement of the shut-state current level at depolarized voltages.

*Slow Blockade of BK Channels by $Sr^{2+}$*

The duration of shut events decreased significantly when activation was augmented with an increase in $[Sr^{2+}]_i$ and membrane voltage in BK channels (Fig. 2, *E* and *F*). Thus, shut events longer than 20 ms became very infrequent when the channel was well activated, for example, with 20 μM $[Sr^{2+}]_i$ at 50 mV (Fig. 3 *C*). However, long shut events were observed when the $Sr^{2+}$ concentration was further increased and a large positive voltage was applied (Fig. 7). Long shut events became obvious when the $[Sr^{2+}]_i$ concentration was 500 μM or higher and the voltage was over 30 mV. The activation of BK channels was nearly saturated at these $[Sr^{2+}]_i$ values and membrane voltages (Fig. 2 *A*). On the other hand, the frequency of these long shut events increased when the membrane voltage or $[Sr^{2+}]_i$ was increased. These findings indicate that long shut events are produced by $Sr^{2+}$ by a mechanism different from activation. Internal $Ba^{2+}$ also produced long shut events in BK channels in the present study (Fig. 7 *D*), as has been reported in other BK channels (Vergara and Latorre, 1983; Miller et al., 1987). In the present study, I analyzed the long shut events produced by $Sr^{2+}$ in the steady state and ex-

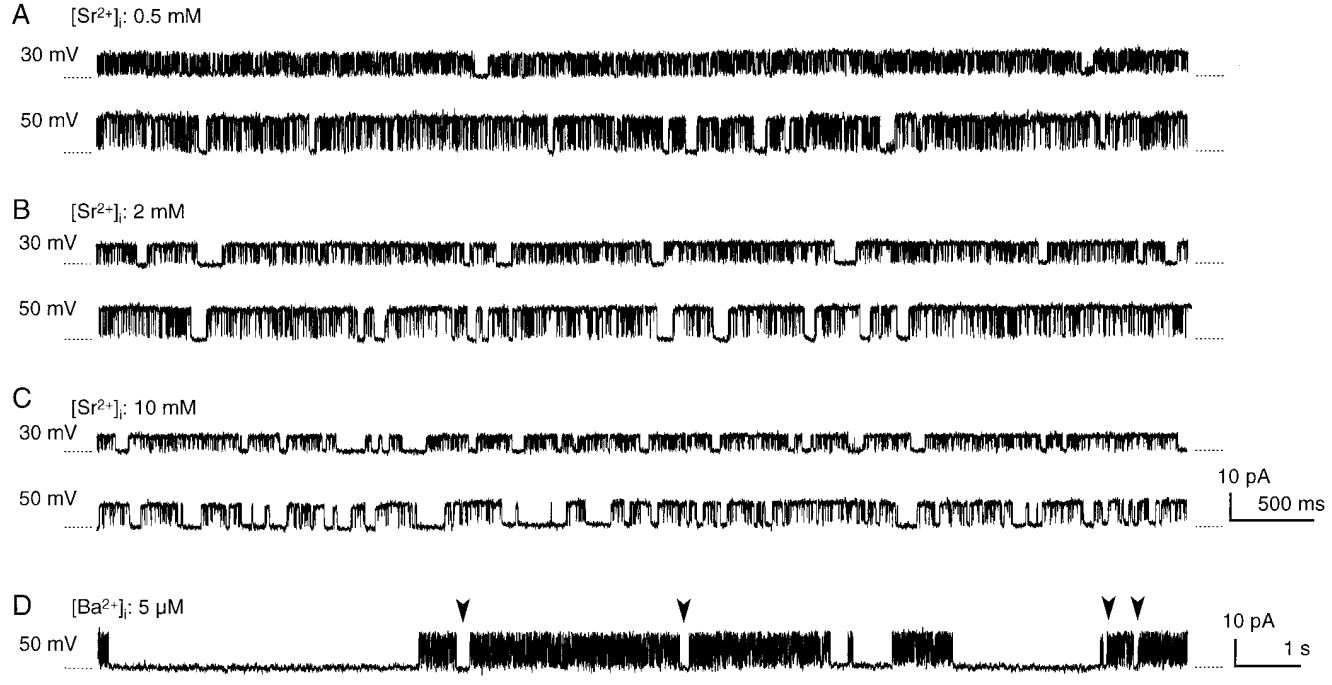


FIGURE 7. Long shut events produced by high $[Sr^{2+}]_i$ and by $[Ba^{2+}]_i$. (*A–C*) Sample records were obtained from a BK channel filtered at 10 kHz and digitized at 20 μs; each 40th point is plotted. Membrane voltage and $[Sr^{2+}]_i$ are indicated for each trace. (*D*) Sample record obtained with 5 μM $[Ba^{2+}]_i$ and 100 μM $[Ca^{2+}]_i$ at 50 mV from a different BK channel. Records were filtered at 10 kHz and digitized at 20 μs; each 100th point is plotted. The zero-current levels are indicated by dotted lines. Arrowheads in *D* indicate some long shut events shorter than 500 ms.

amined whether their mechanism was similar to that of the slow blockade produced by $Ba^{2+}$. Periods of occasional transient shifts in gating were omitted for these analyses (see MATERIALS AND METHODS).

Open- and shut-time histograms were first calculated from continuous records of single BK channels. Sets of histograms based on >34,000 open and shut events were obtained from a membrane patch for different $[Sr^{2+}]_i$ at +30 and +50 mV (Fig. 8). The distributions of open time (Fig. 8, *A–F, row a*) were simple and similar in all cases. Their peak values, which approximately indicated the mean open time, came at ~1 ms in all cases. On the other hand, shut-time distributions were not as simple as open-time distributions. Although most of the shut events were shorter than 20 ms, shut events longer than 20 ms were seen in all cases. Such long shut events were infrequent at 500 μM $[Sr^{2+}]_i$ and 30 mV (Fig. 8 *A, b*). However, with an increase in $[Sr^{2+}]_i$ or membrane voltage, these long shut events occurred more frequently, resulting in the formation of a hump in the time range between 10 and 500 ms in shut-time histograms (Fig. 8, *A–F, row b, arrowheads*). This hump was barely seen with 500 μM and 30 mV (Fig. 8 *A, b*), but became larger with an increase in $[Sr^{2+}]_i$ or voltage (Fig. 8, *B–F, row b*). It was impossible to clearly separate long shut events from ordinary shut events because the hump portion was continuous with the rest of the histogram. However, the transition seemed to occur at ~10–20 ms. A single-exponential distribution (time constant: $\tau_{l-s}$), calculated from bins longer than 20 ms, showed a good fit to the hump portion (i.e., the duration of long shut events) in each shut-time distribution (Fig. 8, *A–F, row b*).

Next, I analyzed the 'burst' duration since its parameters could provide information for analyzing slow

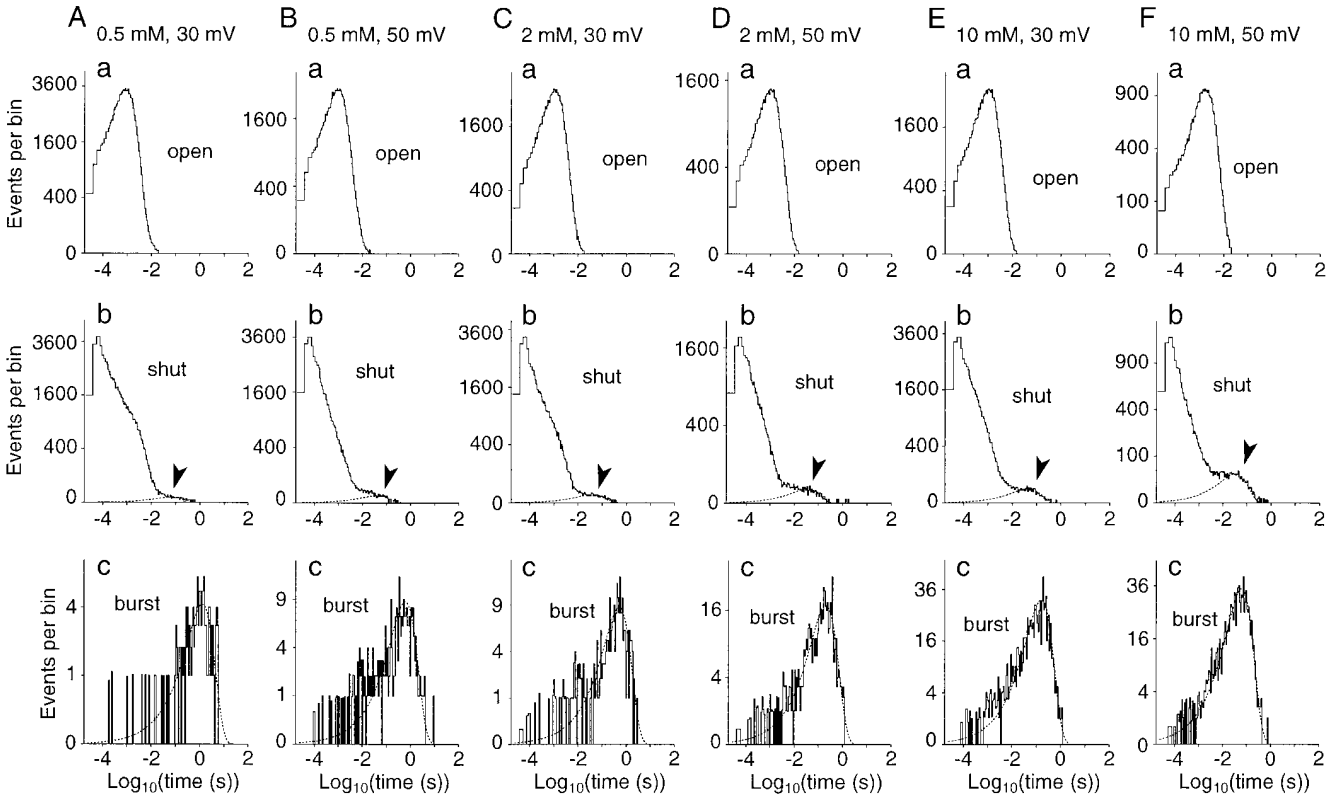


FIGURE 8. Effects of $Sr^{2+}$ and voltage on long shut events shown in histograms of event-duration distributions. (*A–F*) Histograms of open- (*a*), shut- (*b*), and burst- (*c*) time distributions from continuous records obtained from a BK channel at different $[Sr^{2+}]_i$ and membrane voltages (indicated at the top of each column). Arrowheads in *b* indicate the portions of the long shut events (>20 ms) that were fitted with a single exponential (*dotted curve*). To discriminate burst events separated by long shut events, the time at which the number of long shut events shorter than this time equaled the number of ordinary shut events longer than this time was used as a threshold (4.3–16 ms). In *c*, each burst-time distribution was fitted with a single exponential (*dotted curve*). Record length was 156–204 s. Numbers of open, shut, burst, and long shut events, respectively, were 129,288, 129,288, 135, and 136 (0.5 mM, 30 mV); 97,865, 97,865, 275, and 276 (0.5 mM, 50 mV); 92,798, 92,799, 276, and 277 (2 mM, 30 mV); 58,494, 58,494, 580, and 581 (2 mM, 50 mV); 98,887, 98,887, 1,069, and 1,070 (10 mM, 30 mV); 34,052, 34,051, 1,151, and 1,151 (10 mM, 50 mV). The time constants of the exponentials for the duration of long shut events are 75.1, 44.7, 41.3, 41.0, 44.6, and 34.4 ms, respectively, for *A–F*. The time constants of the exponentials for the burst durations are 1,310, 631, 520, 195, 163, and 63.2 ms, respectively, for *A–F*.

blockade. To determine burst events, I arbitrarily defined a threshold time for long shut events (4.3–16 ms). This was the time at which the number of long shut events shorter than this time equaled the number of ordinary shut events longer than this time (Magleby and Pallotta, 1983*b*). The numbers of long shut events and ordinary shut events were given as the area under or above, respectively, the exponential curve fitting the long shut events. The accuracy of this threshold time was not very significant, as will be discussed later. The duration of each burst (i.e., a period bracketed by long shut events as defined by the threshold) was calculated from the recorded data to make a histogram of burst durations (Fig. 8, *A–F, row c*). Each distribution of burst durations could be fitted well with a single-exponential curve (time constant: $\tau_b$). I assumed that this exponential component accounted for burst events separated by long shut events. It was obvious that the number of burst events increased with an increase in $[Sr^{2+}]_i$ and membrane voltage (note the different ordinate scales in Fig. 8, *A–F, row c*), in parallel with the increase in the frequency of long shut events. In addition, the burst time distribution was shifted to the left with an increase in $[Sr^{2+}]_i$ and membrane voltage. For example, the peak of the fitting exponentials (i.e., the time constant) was 1,310 ms for 500 μM $[Sr^{2+}]_i$ at 30 mV (Fig. 8 *A, c*) and 63.2 ms for 10 mM $[Sr^{2+}]_i$ at 50 mV (Fig. 8 *F, c*). The burst time distribution did not depend much on the threshold time for long shut events. For example, in the case of 10 mM $Sr^{2+}$ and 50 mV, the time constant of the fitting exponential curve for burst time was 51.0, 63.2, and 94.0 ms for threshold times for long shut events of 3.32, 6.64, and 15.8 ms, respectively.

With the methods described above, $\tau_{l-s}$ and $\tau_b$ were measured from current records for different voltages and different $[Sr^{2+}]_i$ in three experiments. These time constants were plotted against $[Sr^{2+}]_i$ in log–log coordinates (Fig. 9 *A*). These plots were well-fitted with straight lines (Fig. 9 *A*). It was obvious that $\tau_b$ was strongly dependent on $[Sr^{2+}]_i$ (slopes of the fitting lines: −0.74 to −1.23), and was smaller for higher $[Sr^{2+}]_i$. On the other hand, $\tau_{l-s}$ did not depend much on $[Sr^{2+}]_i$ (slopes of the fitting lines: −0.15–0.01).

Next, I measured the ratio of the occurrence of the long shut state to the occurrence of other shut events ($n_{l-s}/n_s$). This ratio should be the same as the ratio of the occurrence of burst events to that of open events, and is related to the rate constant of the transition from the nonlong to the long shut state. The area under the exponential curve that fit the long shut events

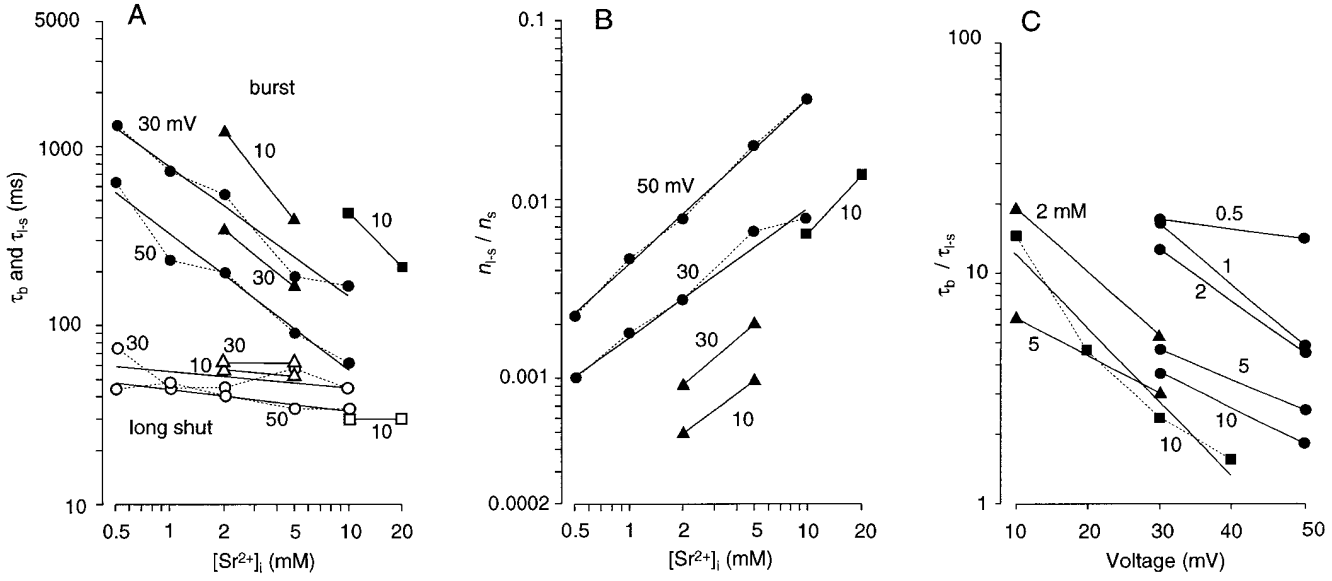


FIGURE 9. Concentration and voltage dependence of the parameters of the burst and slow blocked states. (*A*) The time constants of the exponentials that fit the burst duration ($\tau_b$) (*filled symbols*) and long shut events ($\tau_{l-s}$) (*open symbols*) (see Fig. 8) are plotted against $[Sr^{2+}]_i$. (*B*) The ratio of the occurrence of the blocked state versus other shut states ($n_{l-s}/n_s$) is plotted against $[Sr^{2+}]_i$. This fraction was calculated as the ratio of the area of the single-exponential component that fit long shut events (see Fig. 8, *A–F, row b*) to the total number of shut events counted. (*C*) Ratios of $\tau_b$ versus $\tau_{l-s}$ are plotted against membrane voltage. In *A–C*, different symbols indicate different membrane patches. More than two points obtained from the same membrane voltage in *A* and *B* or from the same $[Sr^{2+}]_i$ in *C* are connected by dotted lines. Membrane voltage (in *A* and *B*) or $[Sr^{2+}]_i$ (in *C*) for each set of points are indicated. The slopes of the lines that fit each set of points: burst in *A*, −0.74 (30 mV, *circle*), −0.74 (50 mV, *circle*), −1.00 (*square*), −1.23 (10 mV, *triangle*), −0.78 (30 mV, *triangle*); slow blocked in *A*, −0.094 (30 mV, *circle*), and −0.11 (50 mV, *circle*), −0.05 (*square*), 0.01 (30 mV, *triangle*), −0.15 (10 mV, *triangle*); $n_{l-s}/n_s$ in *B*, 0.92 (50 mV, *circle*) and 0.71 (30 mV, *circle*), 1.18 (*square*), 1.08 (30 mV, *triangle*), 0.95 (10 mV, *triangle*); $\tau_b/\tau_{l-s}$ in *C*, log($e^{-0.0381}$-fold) $mV^{-1}$ (*circle*, average), log($e^{-0.0737}$-fold) $mV^{-1}$ (*square*), log($e^{-0.0506}$-fold) $mV^{-1}$ (*triangle*, average).

was used as the occurrence of long shut events ($n_{1-s}$) in each shut-time histogram and the number of other shut events ($n_s$) was obtained by subtracting $n_{1-s}$ from the total number of shut events counted. $n_{1-s}/n_s$ was plotted against $[Sr^{2+}]_i$ in log–log coordinates for each channel in each experiment (Fig. 9 *B*). These plots were well-fitted with straight lines, whose slopes ranged from 0.71 to 1.18.

*Interpretation of Slow Blockade Produced by $Sr^{2+}$*

With regard to the mechanism by which long shut states are produced by high $[Sr^{2+}]_i$, I considered the single-site model of Vergara and Latorre (1983), which was originally introduced to explain $Ba^{2+}$-induced blockade (Scheme I), where $\alpha$, $\beta$, $k_1/k_{-1}$ $[Sr^{2+}]_i$, and are rate constants, and $k_1$ and $k_{-1}$ are dependent on voltage but independent of $[Sr^{2+}]_i$. Since this scheme can well explain the occurrence of long shut events, these events will be called slow blocked events (states) in the following analysis. 'Slow' was used to distinguish from fast blockade dealt with in the earlier section. The slow blocked state is represented by 'Blocked,' while 'Shut' and 'Open' were meant to represent all of the open and shut states that occurred during bursts in Scheme I, although there may have been multiple shut and open states. Since flickering gating during bursts (see the previous section on activation) was much faster than the transitions between bursts and slow blocked events, $\alpha$ and $\beta$ should be much larger than $k_1[Sr^{2+}]_i$ and $k_{-1}$. Furthermore, flickering gating during bursts was not significantly affected by the changes in $[Sr^{2+}]_i$ or membrane voltages used in this study of slow blockade due to saturation of activation, as indicated by the following observations. First, distributions of open time, which was an index for $\alpha$, were similar for different $[Sr^{2+}]_i$ and voltages (Fig. 8, *A–F, row a*), indicating that $\alpha$ could be assumed to be unchanged. Second, a very small change in the probability for the open state during bursts ($P$[open|burst]) was observed (0.86 for 500 μM $[Sr^{2+}]_i$ at 30 mV and 0.94 for 10 mM $[Sr^{2+}]_i$ at 50 mV in the case shown in Fig. 8). Thus, $\beta$ could also be assumed to be nearly constant because it was related to $P$[open|burst] and $\alpha$ as follows according to Scheme I:

$$P[\text{open}|\text{burst}] = \beta/(\alpha+\beta). \quad (4)$$

Scheme I predicts that: (*a*) the duration of the blocked state and burst time have single-exponential distributions, (*b*) burst time decreases with increasing $Sr^{2+}$ concentration, and (*c*) blocked time is independent of the $Sr^{2+}$ concentration (Vergara and Latorre, 1983). All of these conditions were approximately satisfied by the experimental results described earlier (Fig. 9, *A* and *B*).

To further assess the validity of Scheme I, relations among $[Sr^{2+}]_i$, $\tau_b$, and $n_{1-s}/n_s$ were deduced. In Scheme I, the burst state stops when the transition

$$\text{Shut} \underset{\alpha}{\overset{\beta}{\rightleftharpoons}} \text{Open} \underset{k_{-1}}{\overset{k_1[Sr^{2+}]_i}{\rightleftharpoons}} \text{Blocked}$$

(SCHEME I)

from open to blocked occurs. Thus, $\tau_b$ can be given by

$$\tau_b = 1/(P[\text{open}|\text{burst}]\, k_1 [Sr^{2+}]_i). \quad (5)$$

Since $P$[open|burst] was nearly constant and $k_1$ is independent of $[Sr^{2+}]_i$, plots of $\log(\tau_b)$ versus $\log([Sr^{2+}]_i)$ should have a slope of $\sim -1$. Meanwhile, $n_{1-s}/n_s$ is determined by the rates of transition from open to shut and open to blocked in Scheme I:

$$n_{1-s}/n_s = [Sr^{2+}]_i\, k_1/\alpha. \quad (6)$$

Since $k_1$ is independent of $[Sr^{2+}]_i$ and $\alpha$ is nearly constant, plots of $\log(n_{1-s}/n_s)$ against $\log [Sr^{2+}]_i$ should have a slope of $\sim 1$. These predictions agreed with experimental measurements (slopes of $\log([Sr^{2+}]_i) - \log(\tau_b)$ plots, $-0.74$ to $-1.23$; slopes of $\log([Sr^{2+}]_i) - \log(n_{1-s}/n_s)$ plots, 0.71–1.18; Fig. 9, *A* and *B*). These results further confirmed the validity of Scheme I for approximating the slow blockade produced by $Sr^{2+}$.

The voltage dependence of the production of $Sr^{2+}$ slow blockade was analyzed using the Woodhull equation, which assumes a single binding site within the membrane voltage gradient in the channel pore for blocking and is compatible with Scheme I:

$$K_{d(S)}(V) = K_{d(S)}(0)\exp(-zdFV/[RT]), \quad (7)$$

where $K_{d(S)}(0)$ is the dissociation constant of the ion for slow blockade at 0 mV, and $z$ and $d$ are as defined in Eq. 2. Based on Scheme I and Eq. 5, $K_{d(S)}(V)$ is related to the burst duration and slow blocked duration as follows:

$$K_{d(S)}(V) = k_{-1}/k_1 = P[\text{open}|\text{burst}]\,[Sr^{2+}]_i \tau_b/\tau_{1-s} \quad (8)$$

Since $P$[open|burst] can be considered a constant (see above), $\tau_b/\tau_{1-s}$ should be proportional to $K_{d(S)}(V)$ under constant $[Sr^{2+}]_i$. As predicted, plots of $\log(\tau_b/\tau_{1-s})$ against membrane voltage at each $[Sr^{2+}]_i$ from several experiments were roughly on straight lines of similar slope, although there was some scattering (Fig. 9 *C*). This indicated that the Woodhull equation (Eq. 7) can account for voltage dependence. In the experiment shown in Fig. 9 *C*, ●, the mean of the slopes of different $[Sr^{2+}]_i$ was $\log(e^{0.0381}\text{-fold})$ $mV^{-1}$, giving a $zd$ value of 0.95 from Eqs. 7 and 8. By extrapolating the plots to a voltage of 0 mV, the value of $K_{d(S)}(0)$ could be calculated. The average $K_{d(S)}(0)$ value obtained from this experiment was 72 mM, using $P$[open|burst] = 0.9. The

values of $K_{d(S)}(0)$ and $zd$ obtained from the two other experiments plotted in Fig. 9 *C* were 36 mM and 1.10 (▲), and 150 mM and 1.84 (■).

Voltage changes affected $\tau_b$ much more than $\tau_{l-s}$, like changes in $[Sr^{2+}]_i$. For example, $\tau_b$ decreased from 425 to 99 ms, while $\tau_{l-s}$ increased from 29 to 63 ms when the membrane voltage was increased from 10 to 50 mV in one case (Fig. 9 *C*, ■). Thus, the voltage dependence of $Sr^{2+}$-induced slow blockade originated mainly from changes in $k_l$ in Scheme I, which should be proportional to the reciprocal of $\tau_b$.

### *Slow Blocked States Produced by Internal $Ba^{2+}$*

Internal barium ion also produced long shut events in BK channels in the present study (Fig. 7 *D*) as has been reported in other BK channels (Vergara and Latorre, 1983; Benham et al., 1985; Neyton and Miller, 1988). The properties of long shut events produced by $Ba^{2+}$ were examined in single BK channels that were almost fully activated by 100 μM $[Ca^{2+}]_i$ at positive membrane voltages. Shut events of long duration occurred frequently with 5 μM $[Ba^{2+}]_i$ at 50 mV (Fig. 7 *D*, note that the time scale is different from those for other traces). These long shut events became frequent with an increase in $[Ba^{2+}]_i$ and voltage (not shown). Some long shut events produced by $Ba^{2+}$ had very long durations (up to several seconds), while other long shut events were shorter than 500 ms (Fig. 7 *D*, *arrowheads*). The duration of the latter was similar to that of long shut events produced by $Sr^{2+}$.

These long shut events were analyzed by making open- and shut-time histograms from records obtained with different $[Ba^{2+}]_i$ (Fig. 10). Shut events longer than 10 ms were rare when no $Ba^{2+}$ was applied (Fig. 10 *A, b*). With 5 μM $[Ba^{2+}]_i$, long shut events of 10 ms–10 s were observed (Fig. 10 *B, b, arrowheads*). With 20 μM $[Ba^{2+}]_i$, the frequency of such long shut events increased, producing an elongated foot in the histogram (Fig. 10 *C, b, arrowheads*). The component produced by long shut events in the shut-time histogram was distributed over such a wide range of time (roughly 10 ms–10 s), which corresponded to the above observations of very and medially long shut events in the current records, that double exponentials, at least, were necessary to achieve a good fit (Fig. 10). On the other hand, the changes due to differences in $[Ba^{2+}]_i$ were small in open-time histograms (Fig. 10, *A–C, row a*). Similar results were observed with internal $Ba^{2+}$ in three other BK channels.

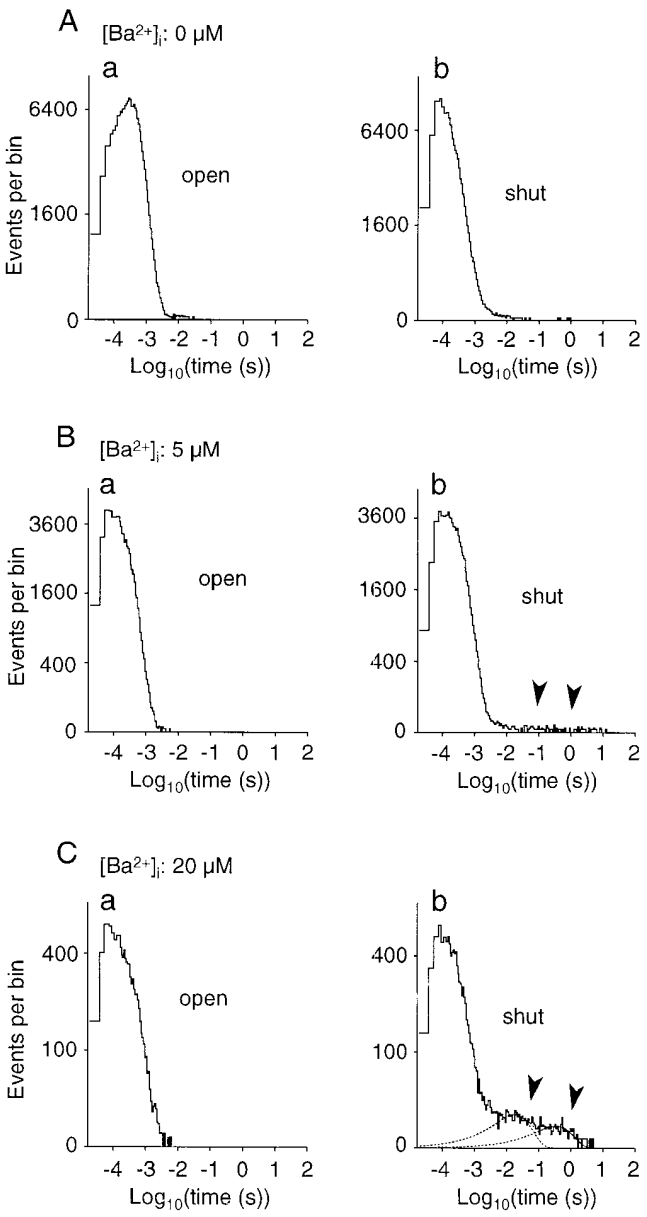


FIGURE 10. Long shut events produced by $[Ba^{2+}]_i$ displayed on event duration distributions. (*A–C*) Histograms showing open- (*a*) and shut- (*b*) time distributions counted from continuous records obtained from a BK channel at different $[Ba^{2+}]_i$, which are indicated at the top. $[Ca^{2+}]_i$ is 100 μM and membrane voltages are 50 mV. In *B* and *C*, arrowheads indicate long shut events produced by $Ba^{2+}$. In *C*, long shut events (>20 ms) were fitted with two exponential curves. Record length: 102–173 s. Numbers of open and shut events: 223,620 and 223,620 (0 μM, 50 mV); 120,247 and 120,247 (5 μM, 50 mV); 16,050 and 16,049 (20 μM, 50 mV). The time constants and area in terms of the number of events for the two exponential curves in *C* are 18.8 ms and 372, and 359 ms and 162, respectively.

## DISCUSSION

Three different effects (i.e., activation, fast blockade, and slow blockade) of internal $Sr^{2+}$ in BK channels in goldfish hair cells were examined in the present study. While only $P_o$ was measured in previous studies on $Sr^{2+}$-induced activation of BK channels (Oberhauser et al., 1988; Yoshida et al., 1991), gatings produced by $Sr^{2+}$ and $Ca^{2+}$ were compared in the present study. The

findings regarding fast blockade produced by $Sr^{2+}$ in the present study were largely similar to the results of a detailed analysis of the fast blockade of skeletal muscle BK channels produced by $Mg^{2+}$ and other divalent cations (Ferguson, 1991). The present study was the first to analyze in detail the slow blockade produced by $Sr^{2+}$.

These different effects produced by $Sr^{2+}$ were apparently independent of each other, indicating that there are specific $Sr^{2+}$-sensitive sites in the channel molecule related to these effects. The activation, fast blockade, and slow blockade sites may be on the cytoplasmic side of the channel molecule, near the internal entrance of the channel pore slightly within the membrane voltage field, and deep in the channel pore under the strong influence of the membrane voltage field, respectively, as discussed below.

### *$Sr^{2+}$-induced Activation of BK Channels*

$Sr^{2+}$-induced activation of BK channels has been reported in skeletal muscle T-tubule membrane incorporated into planar lipid bilayers (Oberhauser et al., 1988) and in isolated hippocampal pyramidal cells of young (7–10 d old) rats (Yoshida et al., 1991). The dose at which $Sr^{2+}$ produced half-maximum activation ($P_o$ = 1/2 $P_{oMAX}$) was 161 and 19.6 times higher than that needed for $Ca^{2+}$, respectively, in the former and latter preparations. In the present BK channel, the concentration of $Sr^{2+}$ needed to produce half-maximum activation was only approximately four times higher than that needed for $Ca^{2+}$. Thus, while the relative potencies of $Sr^{2+}$ and $Ca^{2+}$ for activating BK channels seem to vary among different BK channels, $Sr^{2+}$ is always less potent than $Ca^{2+}$.

It has been assumed that there are several $Ca^{2+}$ binding sites in BK channels (Magleby and Pallotta, 1983*a*; Moczydlowski and Latorre, 1983). The difference in the concentrations of $Sr^{2+}$ and $Ca^{2+}$ necessary to activate the channel indicated that the affinity of $Sr^{2+}$ for $Ca^{2+}$ binding sites is about a quarter of that for $Ca^{2+}$. However, the dose–response curves for $Sr^{2+}$ were less steep than those for $Ca^{2+}$ (Fig. 2 *A*). This was also reflected in the difference between the Hill coefficients for $Ca^{2+}$ and $Sr^{2+}$ (Fig. 2 *B*). A simple explanation for this finding is that the degree of cooperative interaction of ligand binding sites is weaker for $Sr^{2+}$ than for $Ca^{2+}$, in addition to the difference in affinity. A difference in the slopes of the dose–response curves for $Ca^{2+}$ and $Sr^{2+}$ was also observed in skeletal muscle BK channels (Oberhauser et al., 1988).

A major finding of the present study was the close similarity of the activities of BK channels evoked by equipotent concentrations of $Ca^{2+}$ or $Sr^{2+}$, despite the difference in the dose–response curves. Similarity was observed with regard to maximum $P_o$, the voltage dependence of activation, steady state gating kinetics, and the time course of pulse-evoked activation and deactivation of average current. This result is in sharp contrast to the case of the nicotinic acetylcholine receptor cation channel, in which different agonists produce different gating (Colquhoun and Sakmann, 1985). The present results indicated that the same gating scheme can explain both $Ca^{2+}$- and $Sr^{2+}$-induced activation in BK channels. If the main or final activation process is not ligand dependent but rather voltage dependent, it would explain why $Sr^{2+}$ and $Ca^{2+}$ produced indistinguishable activity in BK channels. The difference in the affinity of $Sr^{2+}$ and $Ca^{2+}$ to the binding sites suggests differences in the association and dissociation rates of these cations to the binding sites. The similarity of activity of $Sr^{2+}$- and $Ca^{2+}$-activated channels (Fig. 3) in spite of these differences may suggest the possibility that each open or shut state related to each component in open and shut time histograms does not necessarily correspond to different numbers of ligands bound, but is mostly determined by intrinsic mechanisms.

The voltage and ligand dependence of the activation of BK channels have recently been examined in detail using cloned channels expressed in *Xenopus* oocytes. It has shown that the "tail" domain on the carboxyl side determines apparent sensitivity to the ligand while the "core" domain on the amino side determines open time, conductance, and, probably, voltage dependence (Wei et al., 1994). These authors first argued in favor of independent voltage and ligand steps in the activation process on the basis of the flattening in the $\log([Ca^{2+}]_i) - V_{0.5}$ relation. A study of macroscopic and single-channel current has shown that $Ca^{2+}$ and voltage have distinct effects on activation (DiChiara and Reinhart, 1995). Studies of macroscopic and gating current have demonstrated calcium-independent activation (Meera et al., 1996) and have suggested the presence of voltage-dependent and ligand-independent steps in the activation process (Toro et al., 1996; Stefani et al., 1997). Another study of macroscopic current kinetics indicated the presence of an intrinsic voltage-dependent central activation process (Cui et al., 1997). The results of the present study also support the view that a ligand- and a voltage-sensitive activation process are partially segregated, and that an intrinsic voltage-dependent activation process in BK channels is present.

### *Fast Blockade by $Sr^{2+}$*

The results of this study show that intracellular $Sr^{2+}$ reversibly reduces single-channel current through the BK channel in goldfish hair cells in a voltage- and concentration-dependent manner without changing the zero-current voltage. $Ca^{2+}$ and $Mg^{2+}$ also produced similar current reduction. The potencies of these cations in re-

ducing current amplitude were not very different. A very similar effect has been observed in cultured rat skeletal muscle BK channels for $Mg^{2+}$, $Ni^{2+}$, $Ca^{2+}$, and $Sr^{2+}$ (Ferguson, 1991). However, in cultured neurons from rat hypothalamus and brain stem, the potency of internal $Ca^{2+}$ was ~1,000× higher than that of internal $Mg^{2+}$ in reducing the outward current amplitude (Kang et al., 1994). In BK channels from T-tubule membrane in lipid bilayers, $Ca^{2+}$ was >10× as potent as $Mg^{2+}$ or $Sr^{2+}$ (Oberhauser et al., 1988). Therefore, the present BK channel was similar to the BK channel in cultured skeletal muscle. While the order of potency was $Mg^{2+} > Ca^{2+} > Sr^{2+}$ in the present material, the order in skeletal muscle was $Mg^{2+} > Ca^{2+} = Sr^{2+}$ (Ferguson, 1991). Concerning the speed of blockade, $Sr^{2+}$ and other divalent cations produced no significant increase in the noise level, similar to internal tetraethylammonium (TEA) blockade of BK channels (Blatz and Magleby, 1984; Yellen, 1984), while fast blockade of BK channels by internal $Na^+$ is accompanied by an obvious increase in the noise level in open states (Marty, 1983; Yellen, 1984). The original Woodhull equation could account for the blockade produced by different concentrations of internal TEA (Blatz and Magleby, 1984), whereas a modified Woodhull equation was necessary for the fast blockade produced by internal divalent cations.

It would be reasonable to assume that the site for fast blockade by divalent cations is near the internal entrance of the channel pore within the membrane voltage field based on the blockade of permeation and the small *zd* value. It may be in the vestibule of the channel pore as proposed by Ferguson (1991). The mechanism of fast blockade by divalent cations is not yet fully understood (Ferguson, 1991). Voltage-dependent current reduction at a fixed concentration of divalent cation could be fitted by the Woodhull equation in the present study, as in skeletal muscle BK channels (Ferguson, 1991). Furthermore, the current reduction produced by different $Sr^{2+}$ concentrations could be fitted with a modified Woodhull equation with a Hill coefficient value of ~0.7 in the present study. The scheme of competitive interaction between $Mg^{2+}$ and the permeation of $K^+$ proposed by Ferguson (1991) gives a Hill coefficient of 1, and thus it alone cannot be used to interpret this finding. Although the physical basis for the modified Woodhull equation (i.e., Hill coefficient of <1) could not be determined, there are several possible interpretations.

First, a Debye-Hückel ion–ion interaction of electrolytes can be considered. The activity coefficient (f) of electrolytes decreases with an increase in concentration ([X]), with the relationship $\log(f) = -k[X]^{1/2}$, where the constant k is much larger for divalent ions than for monovalent ions (Bockris and Reddy, 1970). The k value for $CaCl_2$ (in M) is 3.2, calculated from known activity coefficient values (f = 0.8588 and 0.7361 for 0.0018 and 0.0095 M of $CaCl_2$, respectively; Bockris and Reddy, 1970). If the activity predicted by this relationship, $[CaCl_2]\exp(-3.2[CaCl_2]^{1/2})$, is used instead of concentration ([B]) in the original Woodhull equation (Eq. 2), the predicted Hill plot is slightly convex upward with a tangential slope of <1. Between 1 and 10 mM $[CaCl_2]$, the resultant curve could be approximated by the modified Woodhull equation (Eq. 3) with $N = 0.9$.

Second, fast blockade by a two-step reaction instead of a single step can be considered. A simple scheme of single-step blockade (Scheme II) fits the Woodhull equation and a Hill coefficient value of 1. However, another model may be possible in which the blocked state is produced by a certain conformational change that can occur after binding of $Sr^{2+}$ (Scheme III).

In this scheme, all of the rate constants ($k_1$, $k_{-1}$, $k_2$, $k_{-2}$) are large enough for fast blockade, and open* is an open state in which $Sr^{2+}$ is bound at a site that triggers a conformational change for fast blockade. According to Scheme III, the probability for the channel to be in the blocked state ($P_B$) is given by:

$$P_B = 1/[1 + K_{d2}(1 + K_{d1}/[Sr^{2+}]_i)], \quad (9)$$

where $K_{d1} = k_{-1}/k_1$ and $K_{d2} = k_{-2}/k_2$. The predicted Hill plot is given by:

$$\begin{aligned}\log_e([i_O - i_B]/i_B) &= \log_e(P_B/[1-P_B]) \\ &= -\log_e[K_{d1}/\exp(\log_e[Sr^{2+}]_i) + 1] \\ &\quad - \log_e(K_{d2}),\end{aligned} \quad (10)$$

where $\log_e[Sr^{2+}]_i$ and $\log_e([i_O - i_B]/i_B)$ are the coordinates of each data point. Eq. 10 gives a curve convex upward with a tangential slope of <1. When the $K_{d1}$ value is 8 mM, the slope of the curve between 1 and 10 mM $[Sr^{2+}]_i$ is ~0.7. Thus, this model can approximate the experimental results.

$$\text{Open} \underset{k_{-1}}{\overset{k_1[Sr^{2+}]_i}{\rightleftharpoons}} \text{Blocked}$$

(SCHEME II)

$$\text{Open} \underset{k_{-1}}{\overset{k_1[Sr^{2+}]_i}{\rightleftharpoons}} \text{Open*} \underset{k_{-2}}{\overset{k_2}{\rightleftharpoons}} \text{Blocked}$$

(SCHEME III)

*Slow Blockade of BK Channels by $Sr^{2+}$*

The kinetics of the slow blockade of BK channels in goldfish hair cells produced by internal $Sr^{2+}$ could be

interpreted by a model of a single binding site within the membrane voltage field. The same model has been used to successfully explain the slow blockade produced by internal $Ba^{2+}$ in BK channels in various preparations (Vergara and Latorre, 1983; Benham et al., 1985; Miller et al., 1987; Diaz et al., 1996). The depth of the $Sr^{2+}$ binding site within the membrane voltage field from the internal orifice, as indicated by the *zd* value in Eq. 7 divided by 2, was 0.5–0.9 in the present study. This value is consistent with those reported for $Ba^{2+}$ blockade (0.8, Vergara and Latorre, 1983; 0.96, Benham et al., 1985; 0.5–0.7, Neyton and Miller, 1988; 0.92, Diaz et al., 1996). The association rate constant ($k_1$ in Scheme I) was much more voltage sensitive than the dissociation rate constant ($k_{-1}$ in Scheme I) in $Sr^{2+}$-induced slow blockade, as observed for $Ba^{2+}$-induced blockade, suggesting that the peak of the energy barrier that the blocking divalent cation needs to jump is quite near the binding site (Vergara and Latorre, 1983; Diaz et al., 1996). Therefore, it would be reasonable to assume that the site for $Sr^{2+}$-induced slow blockade lies within the channel pore and that the energy barrier between the binding site and the internal surface is near the binding site, as hypothesized for $Ba^{2+}$-induced blockade (Vergara and Latorre, 1983; Neyton and Miller, 1988; Diaz et al., 1996).

Slow blockade in BK channels has also been produced with internal $Ca^{2+}$ (Vergara and Latorre, 1983). However, studies with a specific $Ba^{2+}$ chelator have recently suggested that this blockade is not caused by $Ca^{2+}$ but rather by contamination of the internal solution by $Ba^{2+}$ (Neyton, 1996; Diaz et al., 1996). The slow blockade produced by $Sr^{2+}$ in the present study is not likely due to $Ba^{2+}$ contamination since (*a*) the duration of the $Sr^{2+}$-induced blocked state was different from that of the blocked state produced by $Ba^{2+}$, and (*b*) the amount of $Ba^{2+}$ contamination in $SrCl_2$ should be too small to explain the frequent occurrence of slow blocked events under the presence of $Sr^{2+}$ (see MATERIALS AND METHODS).

In my own analysis of $Ba^{2+}$-induced blockade in BK channels of goldfish hair cells, I found that there were at least two exponential components in the distribution of the slow blocked events produced by $Ba^{2+}$. Therefore, I could not apply a simple kinetics analysis to $Ba^{2+}$-induced blockade, as was used for $Sr^{2+}$-induced slow blockade. Although $Ba^{2+}$-induced blockade was not studied further here, the properties of the blockade were roughly similar to those reported in BK channels in skeletal or smooth muscle preparations (Vergara and Latorre, 1983; Benham et al., 1985; Neyton and Miller, 1988; Diaz et al., 1996), especially regarding the concentration range of $[Ba^{2+}]_i$ ($\sim$10 μM), the duration of the blocked state (up to several seconds), and its dependence on $[Ba^{2+}]_i$ and voltage.

The overall similarity of $Sr^{2+}$- and $Ba^{2+}$-induced slow blockade suggests that the binding site for $Sr^{2+}$ may be the same as that for $Ba^{2+}$. Since the Pauling radius of $Sr^{2+}$ (1.13 Å) is slightly smaller than those of $Ba^{2+}$ (1.35 Å) and $K^+$ (1.33 Å), $Sr^{2+}$ may be able to access the $Ba^{2+}$ binding site. However, the slow blockade produced by $Ba^{2+}$ was more complicated than $Sr^{2+}$-induced slow blockade, as indicated by the fact that the durations of $Ba^{2+}$-blocked events could not be fitted with single-exponential curves (Fig. 10). One possible explanation for this difference is that there may be two $Ba^{2+}$ binding sites within the channel pore, as has been proposed in studies on external $Ba^{2+}$-induced blockade in *Shaker* $K^+$ channels (Hurst et al., 1995) and in smooth muscle BK channels (Sohma et al., 1996). If a model of multiple $Ba^{2+}$ binding sites is applicable to $Ba^{2+}$-induced blockade in BK channels of the present study, $Sr^{2+}$ may bind to one of the multiple $Ba^{2+}$ binding sites. The differences in the concentration range required to produce slow blockade and in the duration of blocked events between $Sr^{2+}$ and $Ba^{2+}$ could be due to differences in the energy levels of the binding sites and the barriers to these cations.

The author thanks Dr. Taro Furukawa for his advice and encouragement regarding this work.

This study was supported by Grants-in-Aid for Scientific Research from the Ministry of Education, Science and Culture of Japan.

*Original version received 30 June 1997 and accepted version received 21 October 1997.*

## REFERENCES

Barrett, J.N., K.L. Magleby, and B.S. Pallotta. 1982. Properties of single calcium-activated potassium channels in cultured rat muscle. *J. Physiol. (Camb.).* 331:211–230.

Baux, G., M. Simonneau, L. Tauc, and J.P. Segundo. 1978. Uncoupling of electrotonic synapses by calcium. *Proc. Natl. Acad. Sci. USA.* 75:4577–4581.

Benham, C.D., T.B. Bolton, R.J. Lang, and T. Takewaki. 1985. The mechanism of action of $Ba^{2+}$ and TEA on single $Ca^{2+}$-activated $K^+$-channels in arterial and intestinal smooth muscle cell membranes. *Pflügers Arch.* 403:120–127.

Blatz, A.L., and K.L. Magleby. 1984. Ion conductance and selectivity of single calcium-activated potassium channels in cultured rat muscle. *J. Gen. Physiol.* 84:1–23.

Bockris, J.O., and A.K.N. Reddy. 1970. Modern Electrochemistry. Vol. 1. Plenum Press, New York. 622 pp.

Colquhoun, D., and B. Sakmann. 1985. Fast events in single-channel currents activated by acetylcholine and its analogues at the frog muscle end-plate. *J. Physiol. (Camb.).* 369:501–557.

Cui, J., D.H. Cox, and R.W. Aldrich. 1997. Intrinsic voltage dependence and $Ca^{2+}$ regulation of *mslo* large conductance Ca-activated $K^+$ channels. *J. Gen. Physiol.* 109:647–673.

Dempster, J. 1993. Computer Analysis of Electrophysiological Signals. Academic Press, Inc., London. 228 pp.

Diaz, F., M. Wallner, E. Stefani, L. Toro, and R. Latorre. 1996. Interaction of internal $Ba^{2+}$ with a cloned $Ca^{2+}$-dependent $K^+$ (h*slo*) channel from smooth muscle. *J. Gen. Physiol.* 107:399–407.

DiChiara, T.J., and P.H. Reinhart. 1995. Distinct effects of $Ca^{2+}$ and voltage on the activation and deactivation of cloned $Ca^{2+}$-activated $K^+$ channels. *J. Physiol. (Camb.).* 489:403–418.

Dodge, F.A., Jr., R. Miledi, and R. Rahamimoff. 1969. Strontium and quantal release of transmitter at the neuromuscular junction. *J. Physiol. (Camb.).* 200:267–283.

Fatt, P., and B.L. Ginsborg. 1958. The ionic requirements for the production of action potentials in crustacean muscle fibres. *J. Physiol. (Camb.).* 142:516–543.

Ferguson, W.B. 1991. Competitive $Mg^{2+}$ block of a large-conductance, $Ca^{2+}$-activated $K^+$ channel in rat skeletal muscle: $Ca^{2+}$, $Sr^{2+}$, and $Ni^{2+}$ also block. *J. Gen. Physiol.* 98:163–181.

Hamill, O.P., A. Marty, E. Neher, B. Sakmann, and F.S. Sigworth. 1981. Improved patch-clamp techniques for high resolution current recordings from cells and cell-free membrane patches. *Pflügers Arch.* 391:85–100.

Hurst, R.S., R. Latorre, L. Toro, and E. Stefani. 1995. External barium block of *Shaker* potassium channels: evidence for two binding sites. *J. Gen. Physiol.* 106:1069–1087.

Kang, J., C. Sumners, and P. Posner. 1994. Calcium-modulated inward rectification of a calcium-activated potassium channel in neurons. *J. Neurophysiol.* 72:3023–3025.

Lang, D.G., and A.K. Ritchie. 1990. Tetraethylammonium blockade of apamin-sensitive and insensitive $Ca^{2+}$-activated $K^+$ channels in a pituitary cell line. *J. Physiol. (Camb.).* 425:117–132.

Latorre, R., A. Oberhauser, P. Labarca, and O. Alvarez. 1989. Varieties of calcium-activated potassium channels. *Annu. Rev. Physiol.* 51:385–399.

Magleby, K.L., and B.S. Pallotta. 1983*a*. Calcium dependence of open and shut interval distributions from calcium-activated potassium channels in cultured rat muscle. *J. Physiol. (Camb.).* 344:585–604.

Magleby, K.L., and B.S. Pallotta. 1983*b*. Burst kinetics of single calcium-activated potassium channels in cultured rat muscle. *J. Physiol. (Camb.).* 344:605–623.

Marty, A. 1981. Ca-dependent K channels with large unitary conductance in chromaffin cell membranes. *Nature.* 291:497–500.

Marty, A. 1983. Blocking of large unitary calcium-dependent potassium currents by internal sodium ions. *Pflügers Arch.* 396:179–181.

McManus, O.B., and K.L. Magleby. 1984. Kinetic properties of single Ca-activated potassium channels activated by strontium ions. *Biophys. J.* 45:306*a*. (Abstr.)

McManus, O.B., and K.L. Magleby. 1988. Kinetic states and modes of single large-conductance calcium-activated potassium channels in cultured rat skeletal muscle. *J. Physiol. (Camb.)* 402:79–120.

Meera, P., M. Wallner, Z. Jiang, and L. Toro. 1996. A calcium switch for the functional coupling between α (*hslo*) and β subunits ($K_{v,Ca}\beta$) of maxi K channels. *FEBS Lett.* 382:84–88.

Miller, C., R. Latorre, and I. Reisin. 1987. Coupling of voltage-dependent gating and $Ba^{++}$ block in the high-conductance, $Ca^{++}$-activated $K^+$ channel. *J. Gen. Physiol.* 90:427–449.

Moczydlowski, E., and R. Latorre. 1983. Gating kinetics of $Ca^{2+}$-activated $K^+$ channels from rat muscle incorporated into planar lipid bilayers: evidence for two voltage-dependent $Ca^{2+}$-binding reactions. *J. Gen. Physiol.* 82:511–542.

Neyton, J. 1996. A $Ba^{2+}$ chelator suppresses long shut events in fully activated high-conductance $Ca^{2+}$-dependent $K^+$ channels. *Biophys. J.* 71:220–226.

Neyton, J., and C. Miller. 1988. Discrete $Ba^{2+}$ block as a probe of ion occupancy and pore structure in the high-conductance $Ca^{2+}$-activated $K^+$ channel. *J. Gen. Physiol.* 92:569–586.

Oberhauser, A., O. Alvarez, and R. Latorre. 1988. Activation by divalent cations of a $Ca^{2+}$-activated $K^+$ channel from skeletal muscle membrane. *J. Gen. Physiol.* 92:67–86.

Ohmori, H. 1985. Mechano-electrical transduction currents in isolated vestibular hair cells of the chick. *J. Physiol. (Camb.).* 359:189–217.

Sigworth, F.G., and S.M. Sine. 1987. Data transformations for improved display and fitting of single-channel dwell time histograms. *Biophys. J.* 52:1047–1054.

Sohma, Y., A. Harris, C.J.C. Wardle, B.E. Argent, and M.A. Gray. 1996. Two barium binding sites on a maxi $K^+$ channel from human vas deferens epithelial cells. *Biophys. J.* 70:1316–1325.

Stefani, E., M. Ottolia, F. Noceti, R. Olcese, M. Wallner, R. Latorre, and L. Toro. 1997. Voltage-controlled gating in a large conductance $Ca^{2+}$-sensitive $K^+$ channel (hslo). *Proc. Natl. Acad. Sci. USA.* 94:5427–5431.

Sugihara, I. 1994. Calcium-activated potassium channels in goldfish hair cells. *J. Physiol. (Camb.).* 476:373–390.

Sugihara, I., and T. Furukawa. 1986. Strontium can activate the Ca-dependent K channel in goldfish hair cell membrane. *Proceedings of the International Union of Physiological Sciences.* 16:444. (Abstr.)

Sugihara, I., and T. Furukawa. 1989. Morphological and functional aspects of two different types of hair cells in the goldfish sacculus. *J. Neurophysiol.* 62:1330–1343.

Sugihara, I., and T. Furukawa. 1995. Potassium currents underlying the oscillatory response in hair cells of the goldfish sacculus. *J. Physiol. (Camb.).* 489:443–453.

Sugihara, I., and T. Furukawa. 1996. Inwardly rectifying currents in hair cells and supporting cells in the goldfish sacculus. *J. Physiol. (Camb.).* 495:665–679.

Toro, L., F. Noceti, M. Ottolia, P. Meera, M. Wallner, R. Latorre, and E. Stefani. 1996. Towards an understanding of how voltage and $Ca^{2+}$ operate in a maxi K channel, *hSlo. Biophys. J.* 70:*A*233. (Abstr.)

Vergara, C., and R. Latorre. 1983. Kinetics of $Ca^{2+}$-activated $K^+$ channels from rabbit muscle incorporated into planar bilayers: evidence for a $Ca^{2+}$ and $Ba^{2+}$ blockade. *J. Gen. Physiol.* 82:543–568.

Wei, A., C. Solaro, C. Lingle, and L. Salkoff. 1994. Calcium sensitivity of BK-type $K_{Ca}$ channels determined by a separable domain. *Neuron.* 13:671–681.

Woodhull, A.M. 1973. Ionic blockage of sodium channels in nerve. *J. Gen. Physiol.* 61:687–708.

Yellen, G. 1984. Ionic permeation and blockade in $Ca^{2+}$-activated $K^+$ channels of bovine chromaffin cells. *J. Gen. Physiol.* 84:157–186.

Yoshida, A., M. Oda, and Y. Ikemoto. 1991. Kinetics of the $Ca^{2+}$-activated $K^+$ channel in rat hippocampal neurons. *Jpn. J. Physiol.* 41:297–315.